AD-A246 835

NAVAL POSTGRADUATE SCHOOL
Monterey, California

THESIS

PRECIPITATION ANALYSES USING SSM/I
MEASUREMENTS FOR SELECTED ERICA CYCLONES

by

Bayani J. Almario Jr.

June, 1991

Thesis Advisor: Carlyle H. Wash

Approved for public release; distribution is unlimited

92-05307

92 3 02 041

REPORT DOCUMENTATION PAGE

1a REPORT SECURITY CLASSIFICATION Unclassified	1b. RESTRICTIVE MARKINGS
2a. SECURITY CLASSIFICATION AUTHORITY	3. DISTRIBUTION/AVAILABILITY OF REPORT Approved for public release; distribution is unlimited.
2b DECLASSIFICATION/DOWNGRADING SCHEDULE	
4 PERFORMING ORGANIZATION REPORT NUMBER(S)	5. MONITORING ORGANIZATION REPORT NUMBER(S)

6a. NAME OF PERFORMING ORGANIZATION Naval Postgraduate School	6b. OFFICE SYMBOL (If applicable) 55	7a. NAME OF MONITORING ORGANIZATION Naval Postgraduate School
6c. ADDRESS (City, State, and ZIP Code) Monterey, CA 93943-5000		7b. ADDRESS (City, State, and ZIP Code) Monterey, CA 93943-5000

8a NAME OF FUNDING/SPONSORING ORGANIZATION	8b. OFFICE SYMBOL (If applicable)	9. PROCUREMENT INSTRUMENT IDENTIFICATION NUMBER

8c ADDRESS (City, State, and ZIP Code)	10. SOURCE OF FUNDING NUMBERS			
	Program Element No	Project No	Task No	Work Unit Accession Number

11 TITLE (Include Security Classification)
PRECIPITATION ANALYSES USING SSM/I MEASUREMENTS FOR SELECTED ERICA CYCLONES

12 PERSONAL AUTHOR(S) Bayani J. Almario Jr.

13a TYPE OF REPORT Master's Thesis	13b. TIME COVERED From To	14. DATE OF REPORT (year, month, day) June 1991	15 PAGE COUNT 81

16 SUPPLEMENTARY NOTATION
The views expressed in this thesis are those of the author and do not reflect the official policy or position of the Department of Defense or the U.S. Government

17 COSATI CODES			18. SUBJECT TERMS (continue on reverse if necessary and identify by block number)
FIELD	GROUP	SUBGROUP	Microwave, SSM/I, Precipitation Retrieval, ERICA, Radar observations, GOES IR imagery

19 ABSTRACT (continue on reverse if necessary and identify by block number)

A recently developed SSM/I exponential rain algorithm is evaluated using passive microwave data from ERICA IOPs 2, 3, 4, and 5. Resulting SSM/I rain analyses were first evaluated with aircraft radar and coastal radar data. SSM/I rain analyses in IOPs 2, 3, and 4 were then used with GOES enhanced IR imagery to determine ERICA cyclones' synoptic rain structure.

The SSM/I rain analysis in IOP 5 compared extremely well with the aircraft radar observations. Maximum SSM/I rain rate areas coincided with the radar intensity observations, but SSM/I rain were somewhat less than inferred by the radar.

The SSM/I rain analyses agreed with the coastal radar precipitation patterns as well. However, SSM/I rain intensities were somewhat less than deduced by the radar charts. The SSM/I rain rate data shows promise to significantly improve analysis of precipitation over the ocean, where conventional data is notably sparse.

20. DISTRIBUTION/AVAILABILITY OF ABSTRACT ☒ UNCLASSIFIED/UNLIMITED ☐ SAME AS REPORT ☐ DTIC USERS	21. ABSTRACT SECURITY CLASSIFICATION Unclassified	
22a. NAME OF RESPONSIBLE INDIVIDUAL Carlyle H. Wash	22b. TELEPHONE (Include Area code) (408) 646-2295	22c. OFFICE SYMBOL MR/Wx

DD FORM 1473, 84 MAR   83 APR edition may be used until exhausted   SECURITY CLASSIFICATION OF THIS PAGE
All other editions are obsolete   Unclassified

PRECIPITATION ANALYSES USING SSM/I
MEASUREMENTS FOR SELECTED ERICA CYCLONES

by

Bayani J. Almario Jr.
Captain, United States Air Force
B.S., San Jose Stae University, 1982

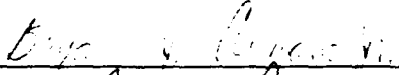Submitted in partial fulfillment
of the requirements for the degree of
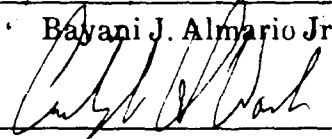
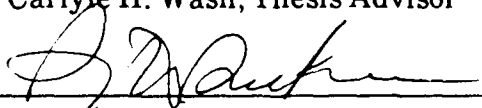MASTER OF SCIENCE IN METEOROLOGY
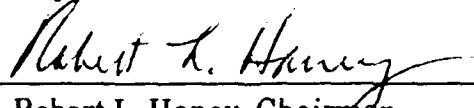
from the

NAVAL POSTGRADUATE SCHOOL
June 1991

Author: _____

Bayani J. Almario Jr.

Approved by: _____

Carlyle H. Wash, Thesis Advisor

_____

Philip A. Durkee, Second Reader

_____

Robert L. Haney, Chairman
Department of Meteorology

ABSTRACT

A recently developed SSM/I exponential rain algorithm is evaluated using passive microwave data from ERICA IOPs 2, 3, 4, and 5. Resulting SSM/I rain analyses were first compared with aircraft radar and coastal radar data. SSM/I rain analyses in IOPs 2, 3, and 4 were then used with GOES enhanced IR imagery to determine ERICA cyclones' synoptic rain structure.

The SSM/I rain analysis in IOP 5 agreed well with the aircraft radar and coastal radar observations. Maximum SSM/I rain rate areas coincided with the radar intensity observations, but SSM/I rain rates were somewhat less than inferred by the radar.

SSM/I rain rate analyses clearly delineate the liquid precipitation patterns within the IOP 2, 3, and 4 cyclones. The SSM/I rain rate data shows promise to significantly improve analysis of precipitation over the ocean, where conventional data is notably sparse.

Accesion For		
NTIS CRA&I		V
DTIC TAB		☐
U..announced		☐
J..stification		
By		
Dist ibution /		
Availability Codes		
Dist	Avail and / or Special	
A-1		

iii

TABLE OF CONTENTS

LIST OF TABLES

LIST OF FIGURES

ACKNOWLEDGMENT

I. INTRODUCTION

The increasing application of satellite data, especially infrared and visible imagery, has greatly enhanced analyses and forecasts of various weather phenomena. One phenomenon that can significantly affect day-to-day air operations is precipitation. Knowing the location and intensity of the precipitation is critical to aviation interests. Despite the useful information obtained from satellite imagery, the infrared and visible radiometers do not directly sense the precipitation. Precipitation estimates from satellite imagery must be complemented with data analyses from synoptic charts and local observations. The use of weather radar, ground-based and aircraft, can also be used to estimate rainfall rate. Numerous empirical studies describe a correlation between a radar's reflectivity factor Z and rainfall rate (Battan 1973). However, precipitation estimates over the vast oceans are uncertain due to inadequate ship and other observations. Ground-based radar measurements of rainfall rates over the ocean are limited to coastal areas due to the radar's effective range of approximately 200 nautical miles (nm). Aircraft radar measurements are quite useful but are rarely available for operational analyses.

One approach to improve oceanic precipitation analysis is the satellite retrieval of precipitation information from passive microwave radiances (Barrett and Martin 1981). This method has the fundamental advantage of penetrating clouds and interacting strongly with precipitation-size drops in liquid phase clouds. Precipitation is therefore directly

detected by the microwave radiation. Most passive microwave data have been made by the Scanning Multichannel Microwave Radiometer (SMMR) on board the Seasat and Nimbus-7 satellites and more recently, by the Special Sensor Microwave/Imager (SSM/I) on the Defense Meteorological Satellite Program (DMSP) satellite. The frequencies used in the retrieval are 18, 21, and 37 GHz from the SMMR and the 19, 22, 37, and 85.5 GHz from the SSM/I.

Over the past several years, numerous investigations using the passive microwave retrieval of precipitation have been conducted. Only a few well-tested, globally applicable algorithms for the estimation of precipitation over the ocean are available. These algorithms include the 85.5 GHz polarization corrected temperature (PCT) algorithm developed by Spencer et al (1989); an algorithm to identify light precipitation using a 19 GHz-22 GHz vertically polarized channel relationship developed by Norman C. Grody (Fiore and Grody 1990); and the algorithm implemented by Katsaros et al (1989) using the 37 GHz horizontally polarized channel to detect precipitation. These algorithms will be discussed in more detail in the next chapter.

Continued study of rain algorithms over the oceans are critical to improve precipitation forecasts for these data-sparse areas. However, verification data are required to demonstrate the effectiveness of the rain algorithms over the ocean. A recent evaluation of the Hughes Aircraft Corporation (HAC) rain algorithm applied on the Experiment on Rapidly Intensifying Cyclones over the Atlantic (ERICA) field study data showed considerable uncertainty in rainfall rate estimation (Cataldo 1990). Large out-of-limits values were evident when the HAC rain algorithm was applied. Analysis of the

directly measured brightness temperatures demonstrated a better overall detection of precipitation.

This thesis will evaluate a new exponential rain algorithm on several ERICA storms in IOPs 2, 3, 4, and 5. This algorithm was developed by a University of Wisconsin team to provide an alternate and improved method to the current Hughes Aircraft Corporation algorithm (Olson et al 1990). The Wisconsin team applied the alternate algorithm to tropical cyclone data and the algorithm produced reasonable rainfall rates estimates comparable to radar data. Studying the ERICA storms with this improved algorithm will determine the effectiveness of the algorithm when applied to mid-latitude cyclones.

The ERICA field study provides a significant amount of verification data for this thesis. ERICA was conducted from 1 December 1988 - 26 February 1989. It was designed to obtain new scientific understanding of the rapid deepening of winter storms at sea (Hadlock and Kreitzberg 1988). The main objectives of the ERICA program were to understand the atmospheric processes occurring in rapidly intensifying storms; determine those processes that must be included into dynamical prediction models; and identify those measurable precursors needed in an initial analysis for improved operational model forecasts.

ERICA-type storms (intensification rate of at least 10 mb/6h for at least 6h) occurred mainly between 35N - 45N along the path of the Gulf Stream. Historically, this region is favorable for occurrence of rapidly deepening storms. To collect data for the ERICA field study, eight Intensive Observations Periods (IOPs) were completed over the winter storms. Actual ERICA-type storms were observed in four IOPs (1, 2, 4, and 5)

3

while two IOPs (3 and 8) had marginal ERICA-type storms. Observations conducted within the IOPs were accomplished using various types of data gathering systems. These systems included aircraft radars and dropwinsondes, rawinsonde soundings, satellite imagery, fixed and drifting buoys, ship report, wind profilers, and ground-based radars.

A literature review of satellite retrieval of precipitation from passive microwave radiance and precipitation algorithms will be presented in Chapter II. Chapter III will provide a detailed comparison of the SSM/I exponential algorithm analyses of the ERICA storms with aircraft and ground-based radar data. Several exponential rain analyses will be compared to corresponding GOES infrared (IR) satellite imagery in Chapter IV. A summary with conclusions and suggestions for future research follow in Chapter V.

II. BACKGROUND

Developing accurate algorithms for precipitation retrieval using passive microwave radiances continues to be an important area of research. Several algorithms have shown positive results in detecting the presence and intensity of precipitation. This chapter describes the basic properties to microwave precipitation retrievals and several recently developed methods to estimate rainfall rates.

A. MICROWAVE PROPERTIES

Passive microwave precipitation retrievals are generally grouped into two different categories, absorption/emission and scattering. The absorption/emission retrieval, used below 20 GHz, depends on emission of passive microwave radiation by the liquid precipitation. The rain drops are observed through these emissions, especially against a radiometrically cold oceanic background (approximately 150°K) due to its low emissivity ($\varepsilon = 0.4$). Microwave brightness temperature, T_B, increases due to microwave emission from the liquid precipitation in this environment since the emissivity of the precipitation is near unity. The brightness temperature can be correlated with rainfall rates to produce rainfall estimation by accounting for the transmittance of a rain layer. As the transmittance of a layer decreases with the obscuration of the surface, the emission of rain dominates the microwave radiance (Kidder and Vonder Harr 1990).

In the scattering-based retrieval, precipitation, especially above freezing level, causes brightness temperature decreases over a radiometrically warm (usually land) background

5

(Spencer et al 1989). The T_B decreases are caused by the presence of ice in the upper levels of the atmosphere. The ice can attenuate upwelling microwave radiation from below the freezing level by scattering photons out of the spaceborne radiometer's field of view (FOV). The microwave radiation measurements above 60 GHz are strongly influenced by scattering by larger water droplets and ice crystals about 60 GHz. This method is less direct in estimating precipitation than the absorption/emission-based retrieval due to scattering rather than emission from rain drops. Between about 20 and 60 GHz, upwelling passive microwave radiation relates to a varying combination of absorption, emission, and scattering.

Fig. 1 illustrates the different effects water and ice have on upwelling passive microwave radiation. In Fig. 1a, dramatic increases in volume scattering occur for both water and ice with increasing frequencies. However, ice has much lower volume absorption than water as depicted in Fig. 1b. The low absorption of microwave radiation by ice leads to high scattering at all SSM/I frequencies (Fig 1c). Therefore, the presence of ice in the atmosphere and the volume scattering for 85.5 GHz is well correlated with high precipitation rates.

Calculating microwave brightness temperature as a function of rainfall rates is determined by using the radiative transfer theory. Figs. 2 and 3 depict the relationship between brightness temperature and rainfall rates for one set of calculations using the frequencies near the SSM/I of 18, 37 and 85.6 GHz.

Fig. 2 shows the difference in the brightness temperature-rainfall rate relationships between land and ocean. There is a rapid increase in T_B at lower rainfall rates due to the
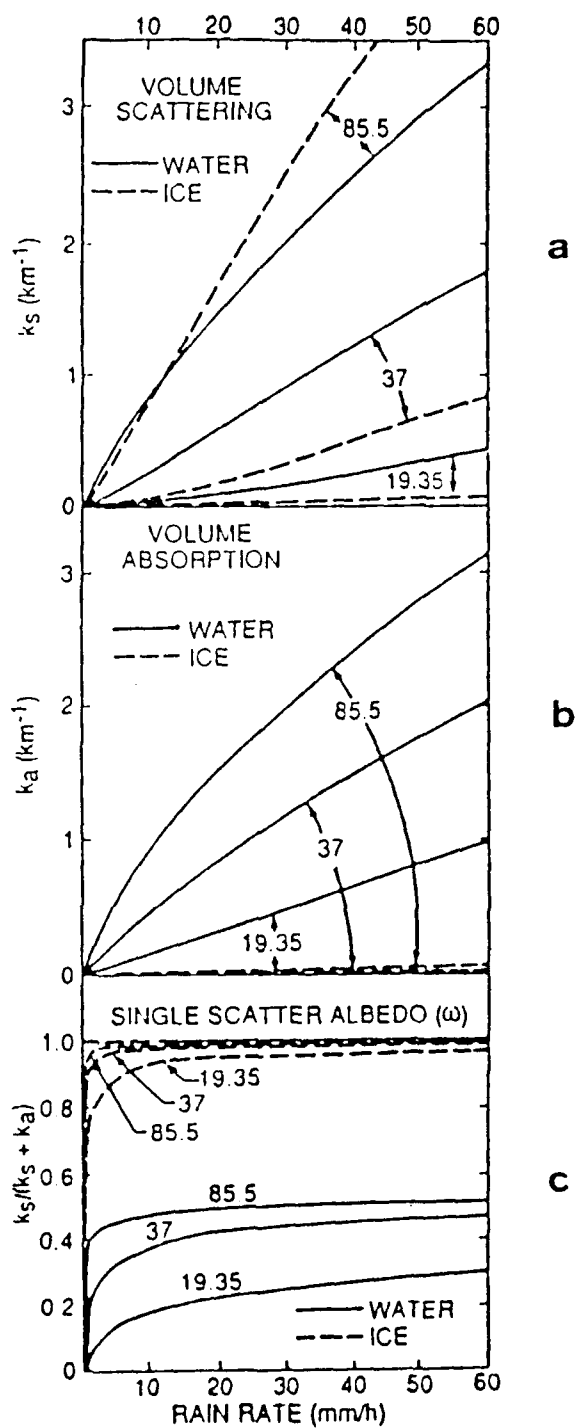
Fig. 1 Mie volume scattering coefficients (a), volume absorption coefficients (b), and single scattering albedos (c) for a Marshall-Palmer precipitation size distribution of water and ice spheres at three frequencies (GHz). [After Spencer et al 1989]

7

large difference in emissivity between raindrops and the ocean. Note that the 18 and 37 GHz frequencies over the ocean are useful only at the low rain rates (less than 20 mm/h). Over land, the emissivity of raindrops and the land are almost the same. The plot shows a decrease in brightness temperature for all three frequencies with increasing rain rates over land due to absorption and scattering by rain. The 85.6 GHz channel depicts the sharpest drop in brightness temperature due to the scattering effect of ice prevalent in higher rainfall rates.

The horizontal and vertical polarizations of the 19 and 37 GHz channels (19H, 19V, 37H, and 37V) depicted in Fig. 3 can also be exploited to detect rainfall rate. Each polarization channel can be used to estimate precipitation, but utilizing both polarization curves simultaneously can also provide rainfall estimation. The plot shows the 19 and 37 GHz frequency polarization channels converging for increasing rain rate. This convergence indicates saturation (surface radiance completely absorbed) is achieved for that specific frequency. The difference between the horizontal and vertical polarizations for a particular rain pixel is related to the intensity of precipitation. The basic properties of passive microwave radiation illustrated above are exploited by several microwave rain rate algorithms.

B.   CURRENT MICROWAVE ALGORITHMS

Several techniques have been developed to utilize the brightness temperature-rainfall rate relationship to produce estimates of rainfall rates. Spencer et al (1989) describes a technique for detecting large ice particles in precipitating clouds using a formulated 85.5

8
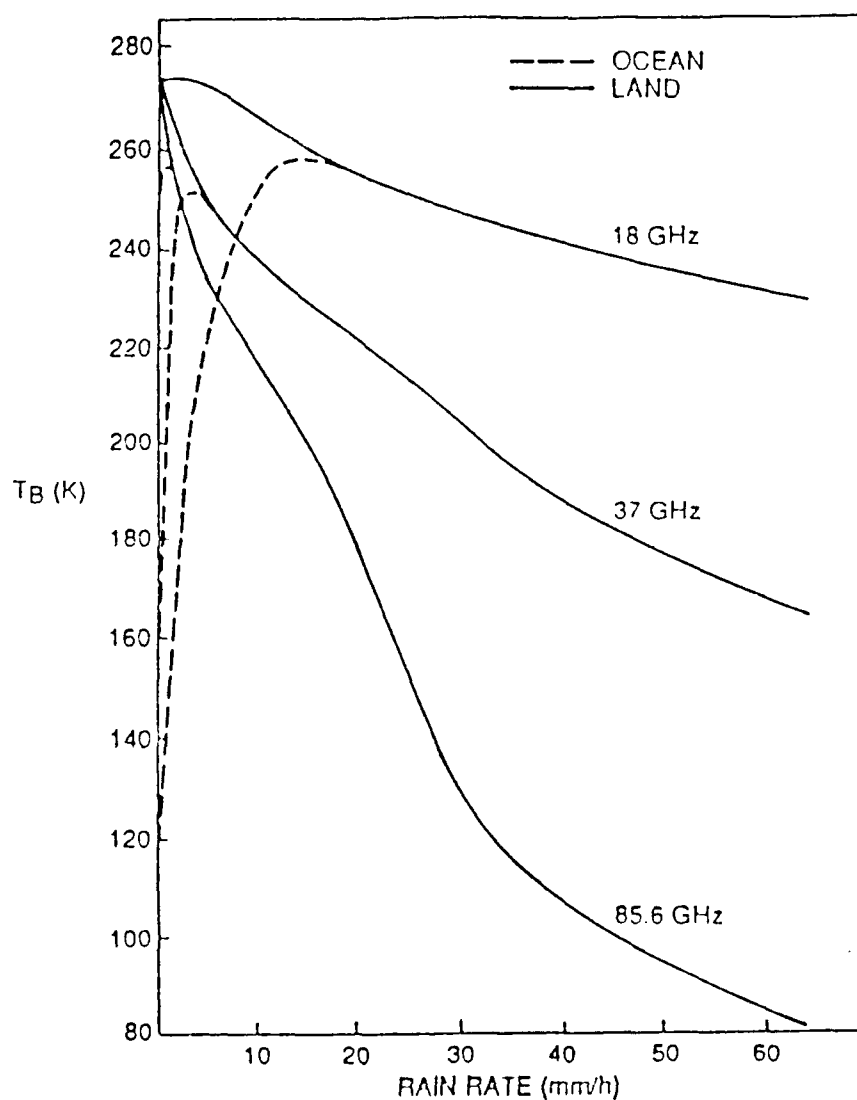
Fig. 2 Brightness temperature versus rain rate for three frequencies. [After Kidder and Vonder Harr 1990]

GHz polarization corrected temperature (PCT) that responds to volume scattering by these particles. The 85.5 GHz PCT equation is

$$PCT = (\beta T_{Bh} - T_{Bv})/(\beta - 1) \qquad (1)$$

9
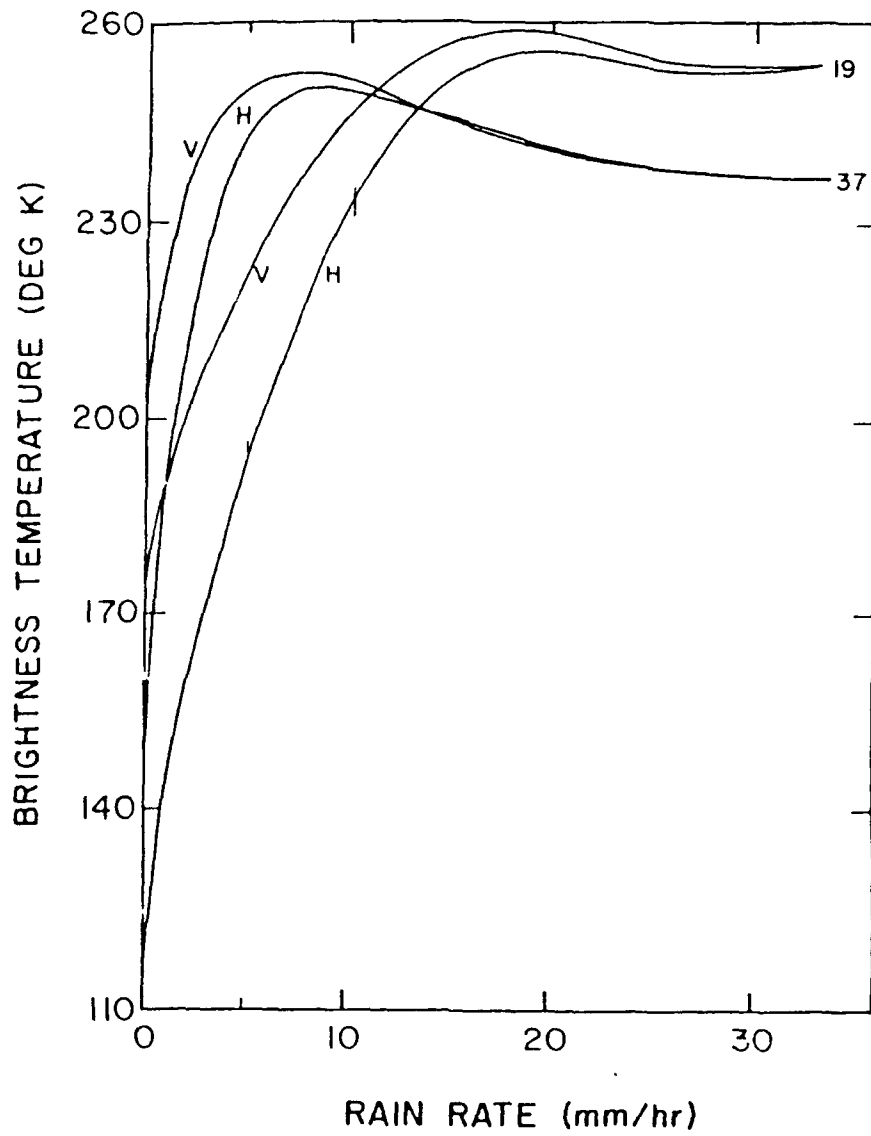
Fig. 3 Mid-latitude ocean brightness temperature versus rain rate at 19 and 37 GHz. [After Hollinger et al 1987]

where

$$\beta = (T_{Bvc} - T_{Bvo})/(T_{Bhc} - T_{Bho}) \tag{2}$$

Here, T_{Bhc} and T_{Bvc} refer to the horizontally and vertically polarized cloudfree ocean T_B, respectively, while T_{Bh} and T_B are horizontally and vertically polarized T_B that are at least

10

partially affected by any combination of clouds and precipitation. T_{Bvo} and T_{Bho} are the vertically and horizontally polarized T_B, respectively, of the ocean with no overlying atmosphere. A PCT threshold of 255°K is suggested for the delineation of precipitation.

Fiore and Grody (1990) formulated an empirical relationship between the SSM/I 19V GHz and the 22 GHz vertically polarized (22V) to identify light precipitation. They separated light precipitation from other scattering materials such as snow cover, sea ice, and glacial ice by using the empirical formula

$$T_B(22V) > 38.0 + .88(T_B(19V). \tag{3}$$

Katsaros et al (1989) used the 37 GHz horizontally polarized channel on the SMMR to flag the presence of precipitation. They used a threshold value of 190°K (Wilheit and Chang 1980) as the rain flag. With the help of a water vapor algorithm, they were able to locate frontal systems over the ocean. Katsaros' rain flag captured the activity near the apex between warm and cold fronts and often shows rain ahead of the warm front. 65 cases were analyzed and produced a 91% success rate in marking frontal zones. The cases that were missed involved weak and complex systems.

The first operational rain algorithm was developed by Hughes Aircraft Corporation using the assumption that there is a linear relationship between brightness temperature and rainfall rate. The HAC algorithm, however, failed to fulfill the specified performance criteria (Hollinger et al 1989). As mentioned earlier, Cataldo (1990) illustrated numerous problems with the HAC algorithm in the study of oceanic cyclone precipitation. Olson

et al (1990) derived a replacement linear regression algorithm using statistical regression of SSM/I brightness temperatures against considearbly more radar rainfall rate observations. The linear regression algorithm showed potential in meeting the specified rain rate criteria. However, these linear algorithms showed a common trend: at low radar-derived rainfall rates, the algorithms tend to overestimate rainfall rate, while at high rainfall rates, they tend to underestimate rain intensity. A more recent algorithm was introduced as an alternate technique by the Wisconsin team (Olson et al 1990). They developed an exponential regression algorithm to account for the nonlinear relationship between the brightness temperature and rainfall rate. Statistical regression analyses were first performed on radar data acquired from Darwin, Australia and Kwajalien. These tropical data were used due to the superior calibration of the radars. Afterwards, simple exponential regression formulas were produced and applied to mid-latitude rain systems. The exponential regression application showed generally superior performance over linear models for mid-latitude systems, although the formulas were based on tropical radar data. The results from these regression analyses contributed to the development of the Wisconsin exponential algorithm.

Before applying the exponential algorithm on SSM/I data, a screening logic has to be satisfied. A negative polarization test is first used to check for bad data. If the equation $(T_B(37V) - T_B(37H))$ or $(T_B(19V) - T_B(19V) - T_B(19H))$ yields values less than -2°K for a particular pixel in a brightness temperature scene, then the pixel is considered not usable.

12

After passing the negative polarization test, if the SSM/I brightness scene includes coastal regions, another empirical function is applied to eliminate false rain signatures near the coast,

$$-11.7939 - .02727T_B(37V) + .09920T_B(37H) > 0. \qquad (4)$$

Different rain algorithms were produced depending on whether the measurement is done over land or ocean and if the 85.5 GHz channel is usable. The following algorithm is used to compute rainfall rate over the ocean and both 85.5 GHz channels (85H and 85V) are usable.

$$R = EXP(3.06231 - .0056036T_B(85V) + .0029478T_B(85H)$$

$$- .0018119T_B(37V) - 00750T_B(22V)$$

$$+ .0097550T_B(19V)) - 8.0 \text{ mm/h}. \qquad (5)$$

When the 85.5 GHz channel is not available, the rain algorithm suggested is

$$R = EXP(5.10196 - .05378T_B(37V) + .02766T_B(37H)$$

$$+ .01373T_B(19V)) - 2.0 \text{ mm/h}. \qquad (6)$$

If the 85.5 GHz horizontally polarized channel is available but not the 85.5V GHz, the following algorithm is recommended.

$$R = EXP(-.42383 -.0082985T_B(85H) + .01496T_B(19V)$$

$$+ .00583T_B(19H)) - 4.0 \text{ mm/h}. \tag{7}$$

The rain algorithm with a usable 85.5H GHz channel (Equation 7) will be used in this thesis on the SSM/I data from the ERICA cases. The 85.5V GHz channel was noisy at this time and its data could not be used.

Olson et al (1990) validated the alternate exponential algorithm using SSM/I data from an overpass of Hurricane Florence on September 10, 1988. Radar-derived rainfall rates obtained from a Louisiana radar station in proximity of the hurricane were used as ground truth. The comparison showed good spatial correlation between SSM/I retrieved rainfall rates and the radar-derived rain rates. Overestimation and underestimation of rainfall rates occurred in certain areas, but overall the SSM/I rainfall rate estimates were reasonable compared with the radar. The improved performance of the exponential algorithm in this tropical case indicates better rainfall rate estimates can be achieved. Evaluation of the exponential algorithm on several ERICA cyclones will be completed in this thesis to study its applicability to mid-latitude rain systems.

III. PRECIPITATION EVALUATION USING RADAR MEASUREMENTS

The use of the meteorological radar is a proven method of remotely sensing precipitation. Its ability to scan rapidly large areas is a major advantage in estimating precipitation. Rainfall rates have been correlated with radar returns using empirical equations which will be discussed later in this chapter. The ERICA data set allows the comparison of SSM/I precipitation estimates with both aircraft and ground-based radar data.

A. COMPARISON OF SSM/I ANALYSIS WITH AIRCRAFT RADAR

One of the most important elements in studying the rapidly intensifying cyclones in the ERICA project was the use of two NOAA WP-3D aircraft. These aircraft provided essential flight-level data (temperature, dew point, wind direction and speed) and dropwinsondes. They also included radar observations from a Doppler radar and a non-Doppler radar. The Doppler radar was located in the tail end of the aircraft, while the non-Doppler radar, which recorded only reflectivity , was situated in the belly of the aircraft (Wakimoto et al 1991). The belly radar will provide the observations for comparison with the SSM/I rain analysis.

1. OPPORTUNITIES FOR COMPARISON OF SSM/I AND AIRCRAFT RADAR DATA

A successful comparison of aircraft radar observations with the SSM/I rain analysis depends on the timing of both SSM/I pass and the aircraft's flight time through

15

the cyclone. The SSM/I coverage (two orbits per day) must be within the aircraft's radar recording period. There were three possible flights that could provide radar data during SSM/I passes for IOPs 2, 3, 4, and 5. Two flights occurred in IOP 4 and the third flight flew during IOP 5. One of the possible flights (Mission OAO #3, 4/0924 - 4/1739 January 1989) in IOP 4 experienced radar problems. The aircraft's radar coverage of the second flight (Mission OAO #2, 4/0021 4/0922 January 1989, was too far from the rain area at the time of the SSM/I pass. The third flight, IOP 5 (Mission OAO #1, 19/0445 - 19/1355 January 1989), provided excellent radar observations and now will be compared with the corresponding SSM/I precipitation analysis.

The P-3 departed on 19/0445 and landed on 19/1355 January 1989. Its overall flight track is presented on Fig. 4. Fig. 5 illustrates the altitude changes of the flight (from 19/0845 to 19/1030) with P-3 recorded wind speed every two minutes at the different levels. The SSM/I pass available during this flight period recorded data starting at 19/0948 January 1989. SSM/I data from 19/0951 to 19/0954 covers the aircraft flight path and this orbit will be now referred to as the 19/0952 January 1989 pass. Fig. 5 shows the P-3 flew at an altitude of about 6700 m from 19/0845 to 19/0935. In the following fifteen minutes, the aircraft descended through the cyclone to an altitude of about 600 m. It maintained this flight level until around 19/1003 where the aircraft further descended to an altitude of 300 m. The concurrent SSM/I pass describes a significant section of the storm and will now be discussed.
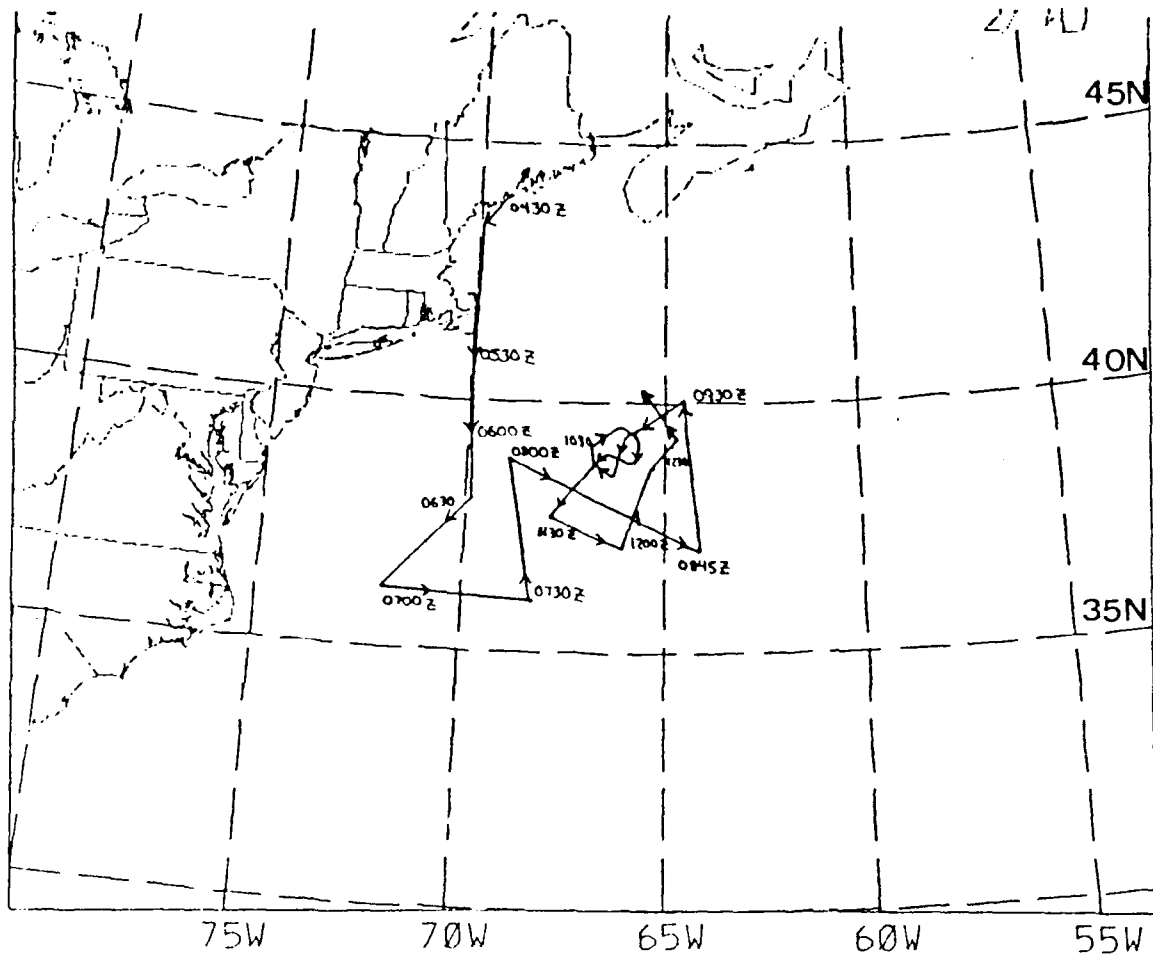
Fig. 4 Flight Track of P-3 Mission OAO #1 on 19 January 1989. [After Hartnet and Hadlock 1989]

2.   19/0952 JANUARY 1989 SSM/I RAIN ANALYSIS

The main precipitation region from the IOP 5 cyclone estimated by the SSM/I is presented in Figs. 6 and 7. Fig. 6 shows the rain analysis using the rain algorithm with the 85.5H GHz channel available (Equation 6). Fig. 7 is the exponential algorithm that did not include the 85.5 GHZ channel (Equation 5). The major difference in the two SSM/I rain analyses are the rain intensities, especially in the maximum rainfall rate areas. Without the aid of the 85.5 GHz channel, higher rainfall rates are not analyzed in Fig. 7.

17
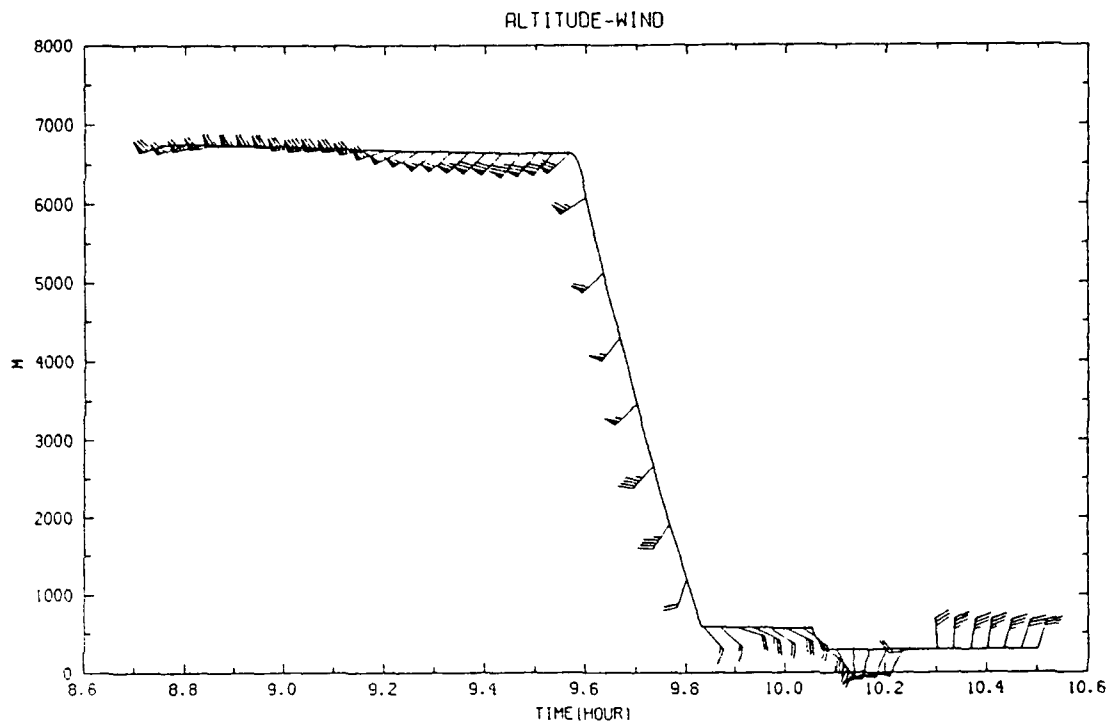
ALTITUDE-WIND

Fig. 5 Altitude-Wind Plot for P-3 Flight 1 during IOP 5. [After Wakimoto et al 1991]

This is reasonable since ice particles and large rain droplets are more prevalent in higher rainfall rates and the 85.5 GHz channel is sensitive to these particles. The aircraft radar can provide confirming evidence on which SSM/I analysis is more realistic.

A segment of the flight track through the storm, from 19/0931 to 19/1020, is overlayed on the rain analysis in Fig 6. The hash marks correspond to radar observation times during the flight that will be used for comparison. The main precipitation area on the 19/0952 rain analysis (Fig. 6) extends south from 41N 66.5W to 34N 68W and eastward to 39.5N 62.5W. A comma head is centered at around 39N 66W with maximum estimated rainfall rates of 9-10 mm/h. A band of precipitation extends due east from the comma head with a cell of maximum precipitation intensities of 9-10 mm/h

18
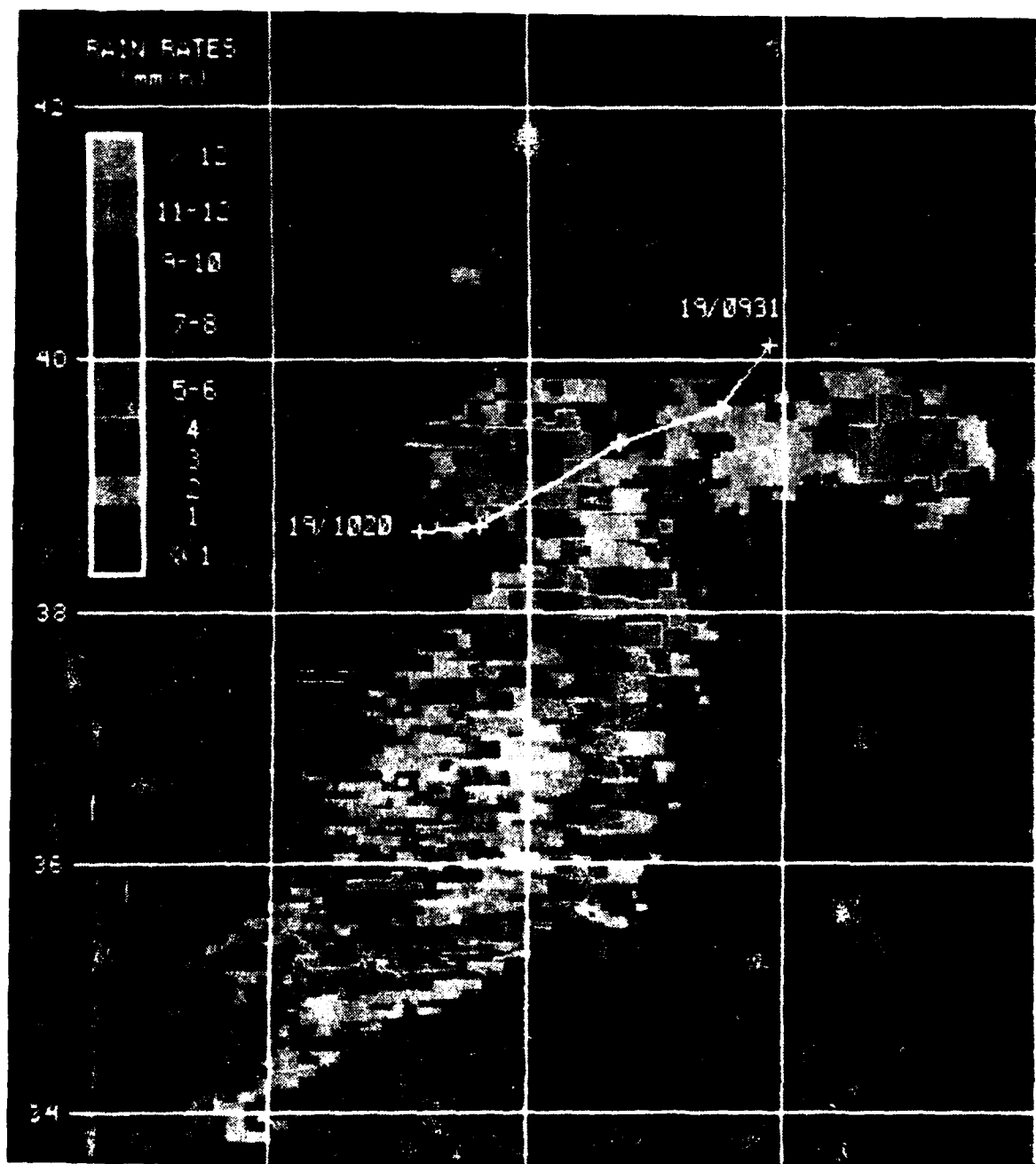
Fig. 6 19/0052 January 1989 SSM/I Exponential Algorithm (85.5H GHz channel included) Rainfall Rate Analysis. Longitude lines are every 2° apart. Western longitude is 68W.

Fig. 7 190052 January 1989 SSM/I Exponential Algorithm (85.5 GHz channel not included) Rainfall Rate Analysis. Longitude lines are 2° apart. Western longitude is 68W.

located at 39.4N 63W. South of the comma head a large region of rain extends south to 34N 68W. Maximum rainfall rates in the middle of this large area are estimated to be greater than 12 mm/h (15 mm/h is the highest rain rate detected). Isolated weaker areas of precipitation are found north of the comma head and slightly west of the southern large rain region. The rain areas are nearly identical in the other SSM/I algorithm (Fig. 7), but the intense rain rate maxima are not resolved.

The precipitation pattern analyzed by the SSM/I exponential algorithm coincides with the comma cloud system depicted in the 19/1001 enhanced GOES IR imagery (Fig. 8). The satellite imagery shows a large area of enhanced high clouds (cloud top temperatures less than 32.2°C) over the cyclone. The high cloud tops are separated into two regions with a gap at around 40N. The southern section of these high clouds covers the comma head and the eastern extension of the SSM/I rain analysis. A comma tail with warmer cloud tops extends southwest from the main mass of high clouds and this tail correlates with the precipitation analysis south of the comma head. The heaviest precipitation terminates at 35.5N in agreement with the southern edge of the colder cloud tops. Interestingly, the northern section of the GOES enhanced cloud top temperature area does not coincide with significant SSM/I rain. No SSM/I precipitation is analyzed over the ocean north of 41N. There were surface reports of drizzle and light rain and snow in this area, but no significant precipitation. A large region of low to middle level clouds cover the Atlantic Ocean east of the cyclone.

3. AIRCRAFT RADAR

The relationship between precipitation intensity and a radar's reflectivity factor Z (Battan 1973) now will be used to interpret aircraft radar. The reflectivity factor Z is a measure of the strength of a target's (e.g. precipitation) backscattering efficiency per unit volume.

As long as the drop-size distribution of the precipitation is known, a reflectivity/rainfall (Z-R) relationship can be made. Since the drop-size distributions are difficult to measure, empirical Z-R relationships have been determined. Most investigators use an empirical expression of the form

$$Z = AR^b, \qquad (1)$$

where R is the rainfall rate in mm/h; Z is the reflectivity factor with units of mm^6/m^3; and A and b are empirically determined constants. Fig. 9 is a plot of the Z-R relationship and two of the most commonly used Z-R relations are depicted on the plot. Marshall-Palmer's equation (1948), $Z = 200R^{1.6}$, is typical for stratiform rain, while Jones' equation (1956), $Z = 486R^{1.37}$, characterizes thunderstorm rain.

Since the values for Z vary over several orders of magnitudes for meteorological observations, Z values are converted to decibels (dB) and expressed as dBZ. The equation for the Z-dBZ relationship is given as

$$dBZ = 10 \log Z. \qquad (2)$$

22
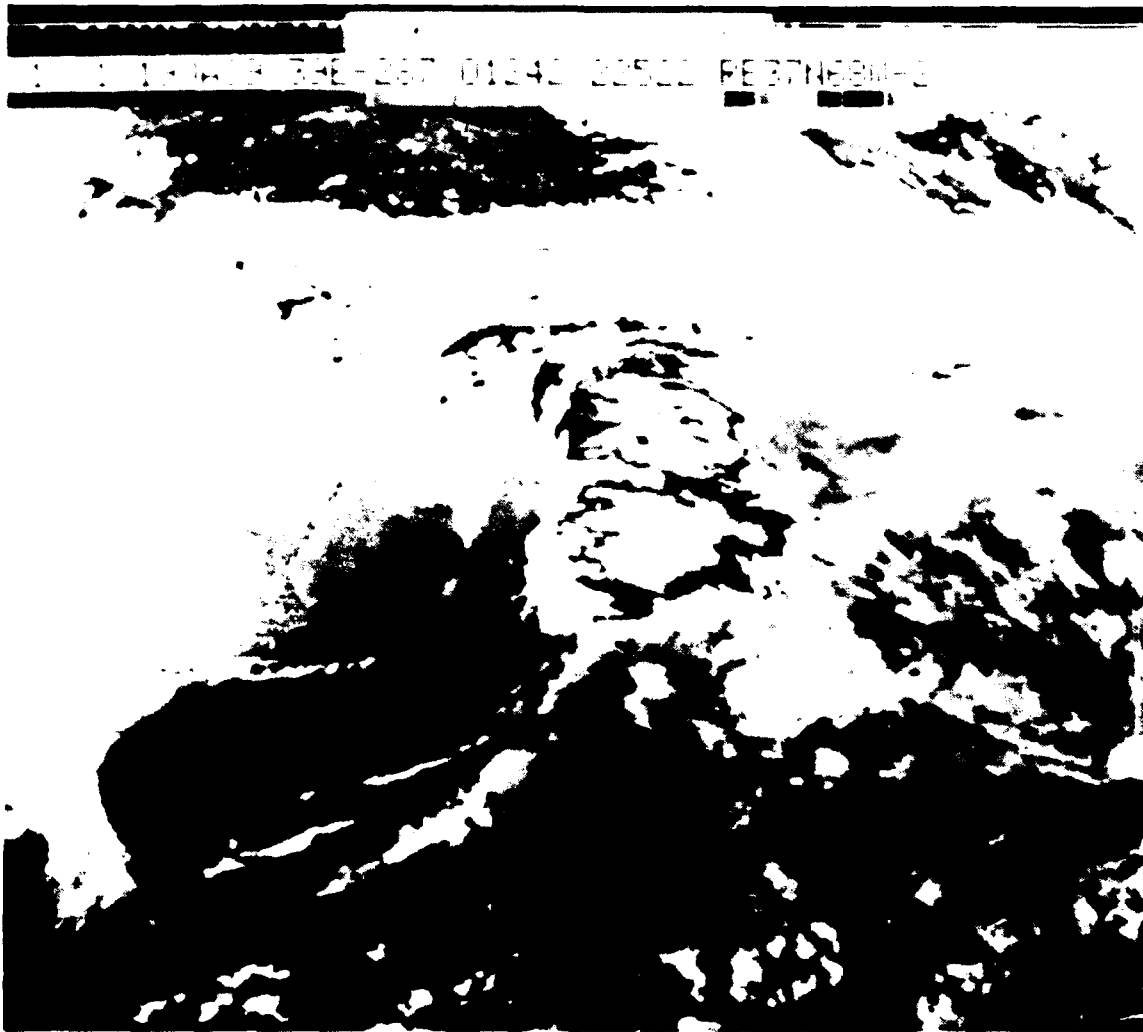
Fig. 8 19/1001 January 1989 GOES Enhanced IR Imagery.

This relationship is important when using radar data since displays of meteorological radar intensity data are normally contours of dBZ (Hembree 1987). The dBZ contours then provide the reflectivity factor Z and an estimate of the rainfall rate.

a. P-3 Aircraft Radar Observations

Many radar observations from the P-3 flight during IOP 5 were processed and converted into reflectivity (dBZ) images. Five radar scenes will be used to study the
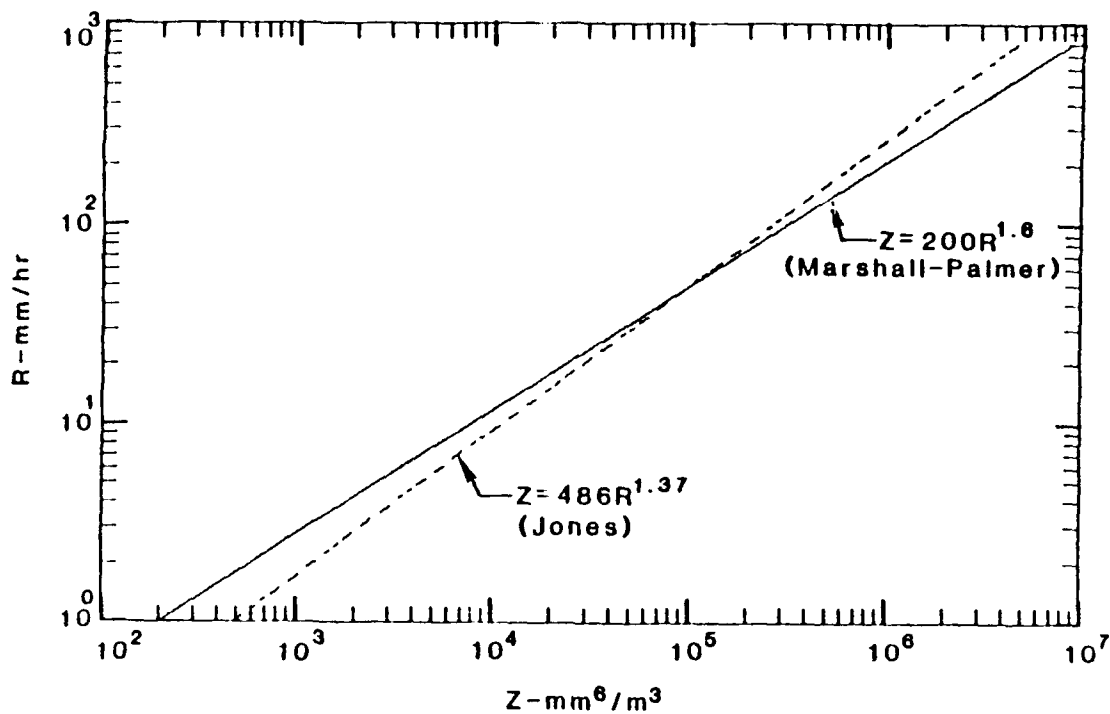
Fig. 9 Plot of two commonly used Z-R relationships. [After Hembree 1987]

19/0948 January 1989 SSM/I rain analysis with observation times of 19/0931, 19/0940, 19/0951, 19/1010, and 19/1020. These times correspond to the flight track hash marks found in Fig. 6.

An attempt to produce a composite radar picture of the main features of the cyclone from the five radar images proved difficult. The time difference between each radar echo pattern allows some intensity and structure changes in the precipitation. The different field of views due to the large aircraft altitude changes contributes to measurements of different intensities for the same cells. Delineating actual precipitation echoes is also difficult due to sea clutter near the aircraft. In light of these difficulties,

it is felt that a detailed comparison of the five radar observations with the SSM/I rain analysis offers more information than a radar composite figure.

b. Comparison of Radar Observations with SSM/I Rain Analysis

The five radar observations selected for comparison with the SSM/I precipitation analysis are within about a half hour of the SSM/I pass. The 19/0931 radar observation (Fig. 10) describes the extent of the precipitation from an altitude of about 6700 m north of the main precipitation regions. At this flight level, radar returns of less than 30 dBZ are prevalent in the scene. Three cells of 30 dBZ and greater are located approximately 150 km southwest (SW), 210 km south-southwest (SSW) and 110 km southeast (SE) of the aircraft. The locations of the two cells SW and SE of the aircraft coincide with the positions of the high rainfall rate cells found in the comma head and the eastward exter ,ir ' of the SSM/I rain analysis (See Fig. 6). The SSW cell appears to be related to the high rainfall rate region found in the upper section of the comma tail.

The SW cell has maximum dBZ values of 32.5 that equates to approximately 5 mm/h on the Marshall-Palmer curve (See Fig. 9). The SSW and SE cells displays returns of 37.5 dBZ or roughly 8 mm/h. The maximum intensities for the corresponding cells on the SSM/I rain analysis are 9-10 mm/h. Since the aircraft is at 6700 m, the radar is sensing only the upper portion of these rain areas. West-northwest of the P-3 are weak radar returns of about 20 to 27.5 dBZ indicating rainfall rates of less than 3 mm/h. This area coincides with the small, isolated region of 2 mm/h rainfall rates north of the comma head. The weakest reflectivity is found north of the aircraft where values are generally less 20 dBZ signifying only a few small precipitation cells. The

25
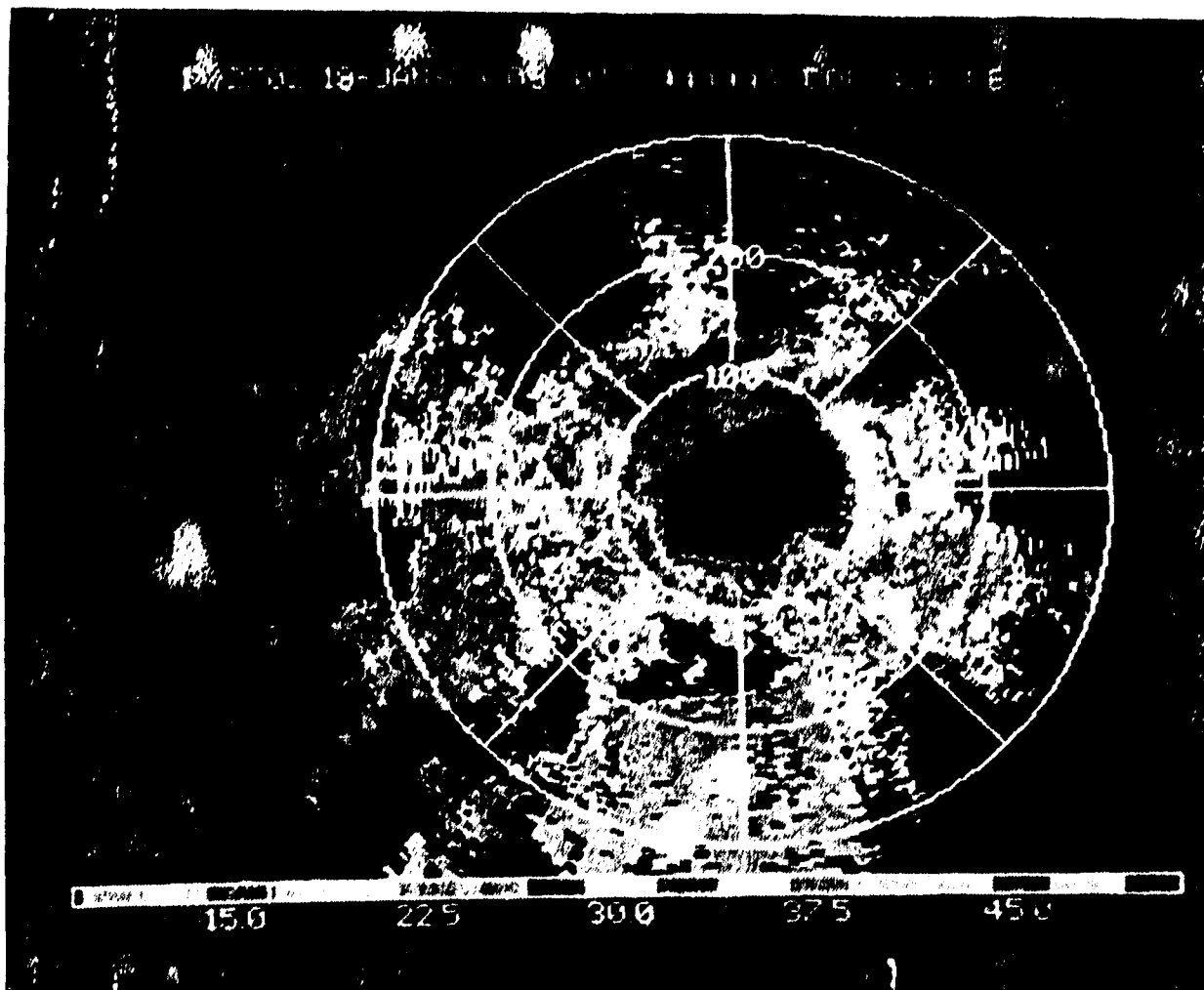
Fig. 10 19/09.31 January 1989 Radar Observation of IOP 5 cyclone.

SSM/I rain analysis also shows no precipitation to the north of the aircraft, even though the cold cloud top temperatures are present. The SSM/I and aircraft radar are the most different south of the aircraft. The SSM/I analysis shows a rain band south of the aircraft joining the eastern and western rain rate maxima. The radar data also suggest a band of light rain activity approximately 100 km south of the P-3. A second larger area of rain is analyzed 200 km southwest to 170 km south of the aircraft. The western section of this area is in agreement with a significant SSM/I rain rate maximum area farther to the

26

southwest. However, the radar rain signature due south of the aircraft are not depicted by the satellite analysis.

For the 19/0940 radar observation (Fig 11), the P-3 was descending into the cyclone and the flight level at this time was about 4300 m (See Fig. 5). This view is only 11 to 14 minutes prior to the SSM/I pass. As the aircraft descends and travels nearer to the comma head, larger radar rain rates are observed.
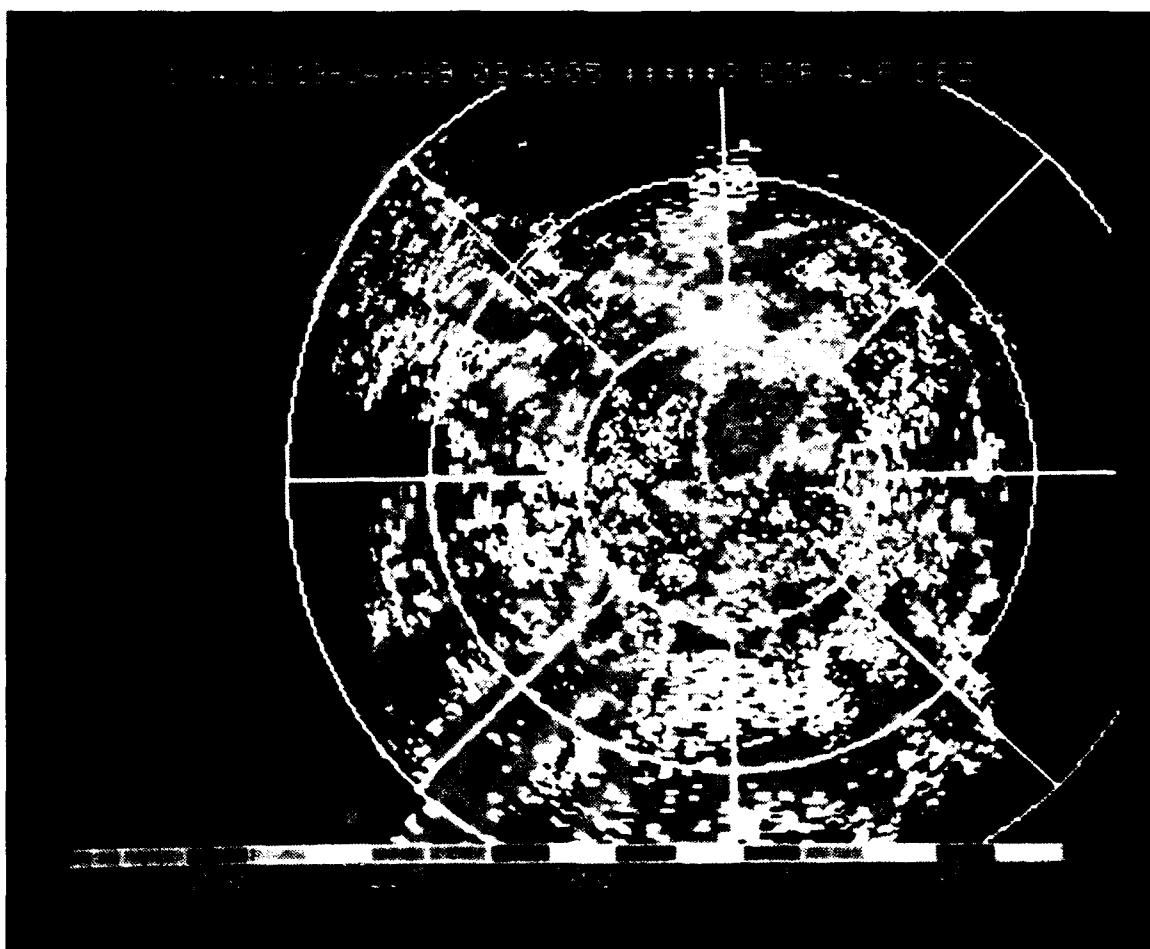
Fig. 11 19/0940 January 1989 Radar Observation of IOP 5 Cyclone.

Three distinct areas of high dBZ values are evident within the large circular pattern of echoes. By noting the aircraft's southwest descent into the storm, it

can be seen that these three regions have emerged from the three smaller areas discussed on the 19/0931 radar scene. The leading edge of the three areas nearest the aircraft are estimated to be 90 km away to the west, 80 km to the east and about 110 km to the south. The distances are approxima' due to inc'easing sea clutter near the aircr..ft.

The t ..d east cells clearly correlate with the SSM/I rain analysis. The leading edges of high rainfall rates west and east of the P-3 position are about one degree longitude (roughly 85 km) from the aircraft. The west cell has maximum dBZ values of 37.5 dBZ (approximately 9 mm/h) whereas the SSM/I rain analysis suggests rates of 9-10 mm/h. Maximum values of 40 dBZ (approximately 11-12 mm/h) are found in the east cell, while rainfall rates of 9-10 mm/h are analyzed by the satellite algorithm. The protruding area of weak echoes (less than 30 dBZ) in the northwest quarter of the radar scene can be reliably related to the small area of light rain north of the comma head.

About 200 km southwest of the P-3, radar echoes of 30 dBZ have emerged indicating observations of the comma tail. Cells south of the aircraft agree with the aircraft moving through the west-east SSM/I precipitation band. Approximately 110 km south of the aircraft is a large area of radar echoes with maximum values of 40 dBZ. Only the extreme western portion of the above-mentioned radar echo area can be correlated with SSM/I rain analysis where rainfall rates of 5-6 mm/h are detected. The echoes south of the aircraft do not match the SSM/I rain rate figure.

By 19/0951, the P-3 is flying at an altitude of 900 m near the comma head. Large sea clutter return is evident in this radar observation (Fig. 12). Due to the

28

sea clutter, defining the edges of maximum radar intensities near the aircraft is impossible. However, the radar shows an area to the west with maximum intensity of 40 dBZ (approximately 12 mm/h). This echo area corresponds to maximum SSM/I rain rate region in the comma head. Examining the next two radar scenes will better define this region.

The general structure of the other precipitation patterns on the radar image strongly follow the SSM/I rain analysis. The extension of radar echoes to the east continues to about 280 km and parallels the west-east band on the SSM/I rain analysis. In the northwest quadrant, the weak rain cells are still present. South-southwest of the radar center, a region of maximum dBZ values (35 to 37.5 dBZ) is depicted. The leading edge of this region is about 100 km from the aircraft. The SSM/I exponential algorithm captures this precipitation area located in the northern section of the comma tail where rain rates reach as high as 11-12 mm/h. With the continuing westward movement of the P-3, the radar rain areas obs' ved due south of the aircraft on the two previous radar scenes should be located approximately 110 km southeast of the P-3. However, the 19/0951 radar observation does not show any precipitation in this area. The disappearance of this rain area cannot be fully resolved at this time and must be investigated further.

The last two radar observations (Figs. 13 and 14) observe the two western high precipitation areas. Both scenes show a circular area of sea clutter since the aircraft is close to the sea surface at these times. The two views reveal two separate regions of maximum radar intensities located north-northeast (NNE) and southeast (SE) of the

29
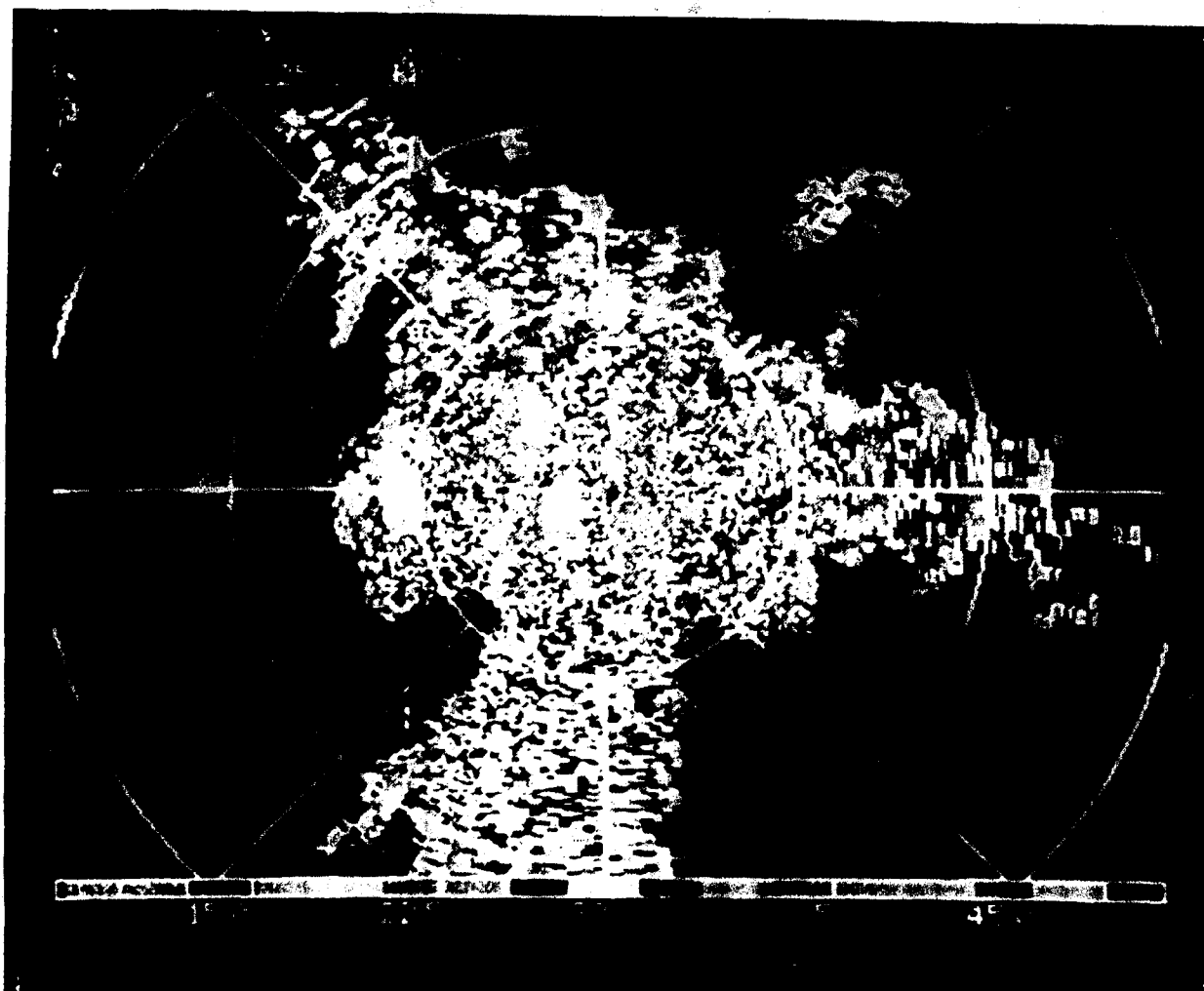
Fig. 12   19/0951 January 1989 Radar Observation of IOP 5 Cyclone.

aircraft position. The NNE sector changes in shape between the two views but they both indicate maximum dBZ values of 40 dBZ (approximately 11-12 mm/h).

The SE sector has similar maximum radar intensities (40 dBZ) as the NNE sector with estimated rainfall rates of 12 mm/h. Taking into account the position of the aircraft and the movement of the cyclone, this sector is related to the northern portion of the comma tail of the SSM/I rain analysis where maximum rainfall rates are 11-12 mm/h. This sector becomes more distinct from the sea clutter in the 19/1020 scene as the aircraft moves westward.
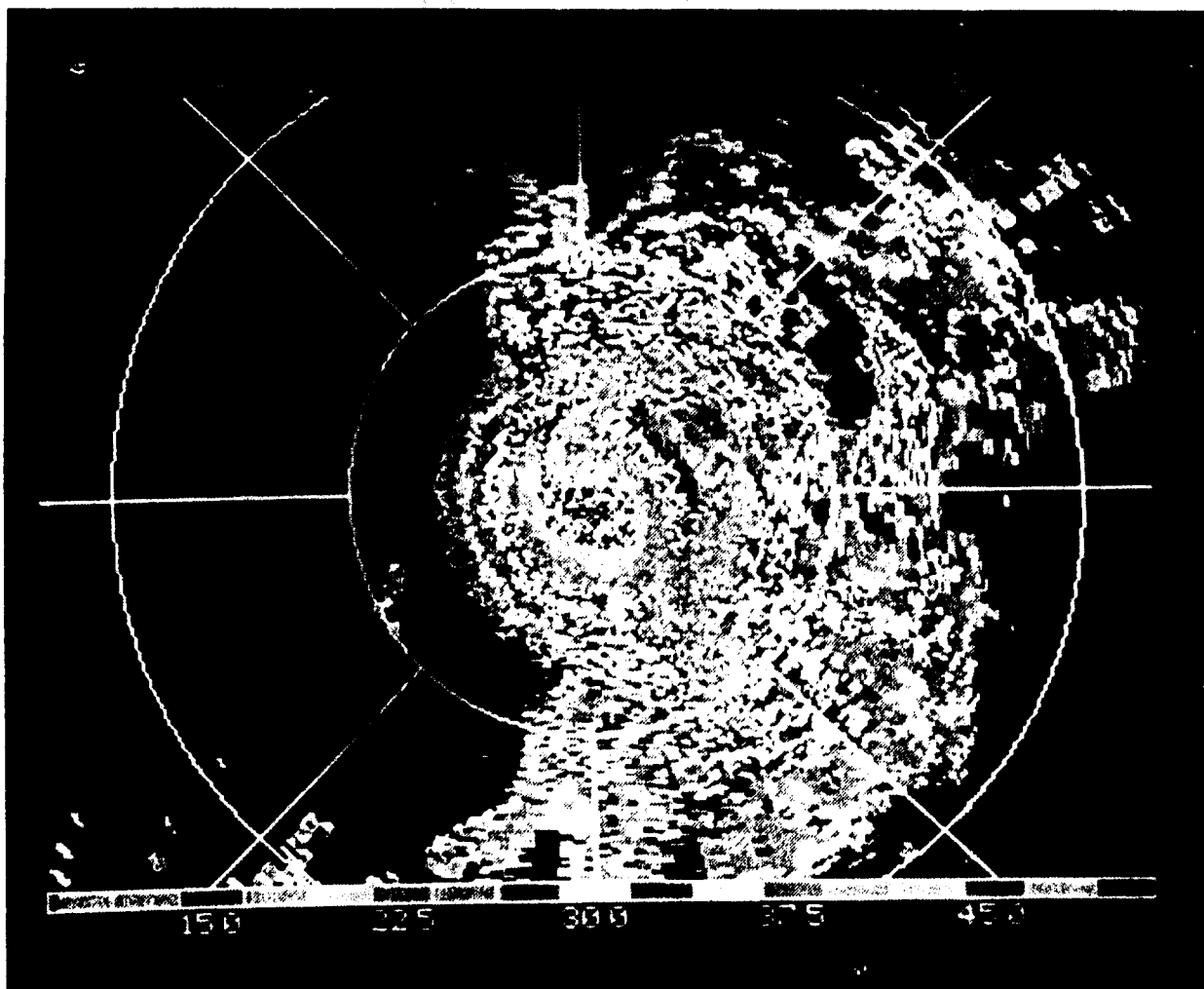
Fig. 13 19/1010 January 1989 Radar Observation of IOP 5 Cyclone.

c. Comparison Summary

The rain/no rain structure of the SSM/I analysis correlates extremely well with the aircraft radar data. Leading edges of maximum rainfall rates from both precipitation patterns are found to be in close agreement. The SSM/I rain rates in these maximum rain areas are strongly correlated to the aircraft radar. The SSM/I analysis for the comma head detected maximum rainfall rates of 9-10 mm/h while the radar reflectivity patterns determined the rainfall rates to be approximately 12 mm/h. The other analyzed maximum rain areas are within 2 mm/h of the radar intensity observations.

31
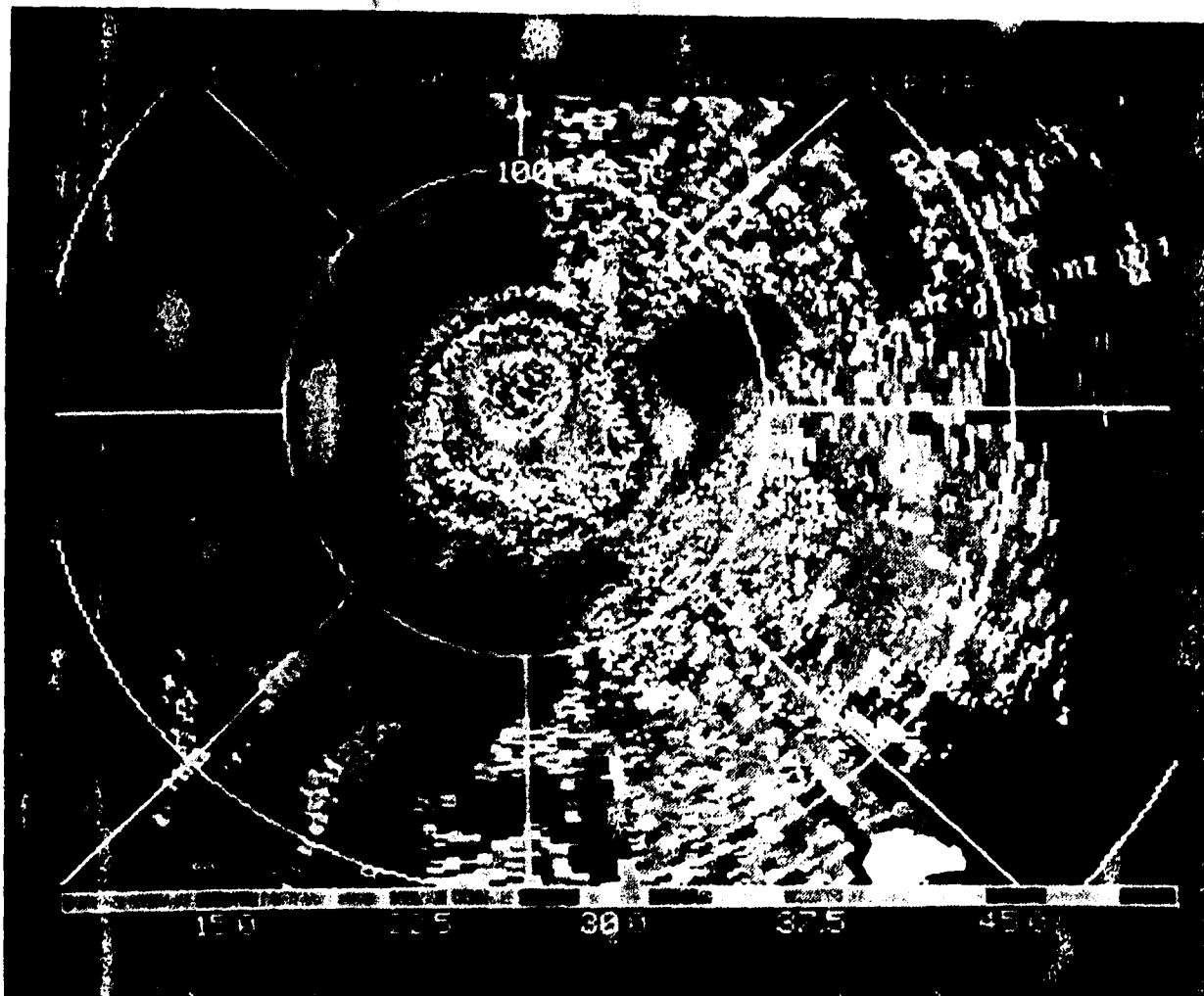
Fig. 14 19/1020 January 1989 Radar Observation of IOP 5 Cyclone.

Even the weak precipitation area projecting north-northwest of the comma head was observed.

There was disagreement between two radar observations (19/0931 and 19/0094 January 1989) and the southern region of the SSM/I rain analysis. The 19/0931 and 19/0040 radar observations showed a rain area due south of the aircraft not directly linked to SSM/I rain analysis. However, this rain area did not appear on the next radar observation (19/0951 January 1989) where the P-3 descended from 4300 m to 600 m. Additional study is needed to explain the disappearance of the rain area between 19/0040

32

and 19/0951 January 1989. With exception of the above area, the aircraft radar-SSM/I rain rate comparison was very successful.

B. COMPARISON OF SSM/I ANALYSIS WITH RADAR SUMMARY CHARTS

The majority of the cyclones in the ERICA field study developed along the eastern U.S. coast. The proximity of the developing cyclones to the coast allow ground-based radar coverage of the storms during the early development periods. Although the operational radar data are analog, radar reports are encoded in digital format using six levels of radar reflectivity, processed by computer at NMC, and converted to facsimile charts. An hourly facsimile chart produced at the National Meteorological Center (NMC), called the Automated Radar Summary (ARS) Chart, provides an analysis of precipitation extent over the United States and coastal waters.

The presence of precipitation is described on the radar summary chart as shaded areas. Six levels of rain intensity are prepared in Table 1 (Sadowski 1979). Contours for echo intensity levels 1, 3, 5 are used on the radar summary charts to distinguish the various levels of precipitation activity. Level 1 indicates rainfall rates of 1 to 3 mm/h; intensities greater than 13 mm/h are contoured as level 3; and level 5 depicts rainfall rates above 114 mm/h. If a level 1 contour is drawn without a level 3 or 5 present within the contour, the precipitation intensity can be either level 1 or 2. These digitized radar data have horizontal resolutions of 20 x 20 nm. The radar summary charts must be used carefully since the coarse resolution of the data will indicate more precipitation than

33

observed. The raw digital values were not available for analysis. These radar summary charts will be compared with relevant SSM/I passes in IOPs 2 and 4.

Table 1   AUTOMATED RADAR SUMMARY PRECIPITATION LEVELS AND THEIR RESPECTIVE RAINFALL RATES. [After Sadowski 1979]

Level of Precipitation	Rainfall Rates (mm/h)
1	1 - 3
2	3 - 13
3	13 - 25
4	56 - 114
5	114 - 180
6	> 180

1.   OPPORTUNITIES FOR COMPARISON

There are four SSM/I precipitation analyses from IOPs 2 and 4 in the coastal zone that can be evaluated with the radar summary charts. One SSM/I pass is from IOP 4 (3/2333 January 1989) and three passes are from IOP 2 (12/2303, 13/0904, and 13/2258 December 1988). The ground-based radar reports on the ARS charts are ¬ited to approximately 220 kilometers (km) (Hembree 1987) which is the effective range of most radars. Thus, the ARS charts can only be used for comparison when precipitation is present within two degrees latitude from the coast.

2.   SSM/I RAINFALL RATE ANALYSIS AND RADAR SUMMARY

a.   SSM/I Data for 3/2333 January 1989

The 3/2333 SSM/I precipitation analysis, Fig. 15, shows an e ¬ensive area of precipitation off the eastern U.S. coast between 31N and 37N. The rain analysis

34

presents a comma-shape feature stretching from North Carolina to Georgia. A one degree sector of missing data is present along 30N-31N. This precipitation area was associated with the development of the intense IOP 4 cyclone. The northern section of the area at around 36N extends inland, while the central section is about one degree away from the coast. The southern section shows the precipitation extending towards the coast.

The SSM/I analysis reveals four distinct cells of high rainfall rates within the precipitation region. One cell is centered at 35N 73.5W and has maximum rainfall rates of 9-10 mm/h. About 36N 73W, an elongated cell is analyzed with maximum intensities of 7-8 mm/h. The other two cells are located in the lower section of the precipitation region along 33N. The two cells parallel each other in northeast-southwest orientation. Both have maximum rainfall rates of 7-8 mm/h positioned in the center of the individual cells.

b.   Radar Summary Chart for 3/2335 January 1989

A comma-shape pattern of precipitation is also depicted on the 3/2335 radar summary chart (Fig. 16) that is nearly the same time as the SSM/I pass. The precipitation extends from 41N to around 31N that includes snow and snow showers in the northernmost part of the region. Available surface observations at 3/2300 and 4/0000 indicate the snow and snow showers occurred north of 38N with predominantly rain and rain showers in the rest of the precipitation area. Isolated thundershowers are found along the tail end of the comma-shape pattern.

The general rain/no rain structure of the SSM/I precipitation analysis corresponds very well with the radar summary chart. The comma-shape pattern is evident

Fig. 15   3/2333 January 1989 SSM/I Exponential Algorithm Rainfall Rate Analysis. Latitude and Longitude lines are 10° apart. Southern latitude is 30N and western longitude is 80W.
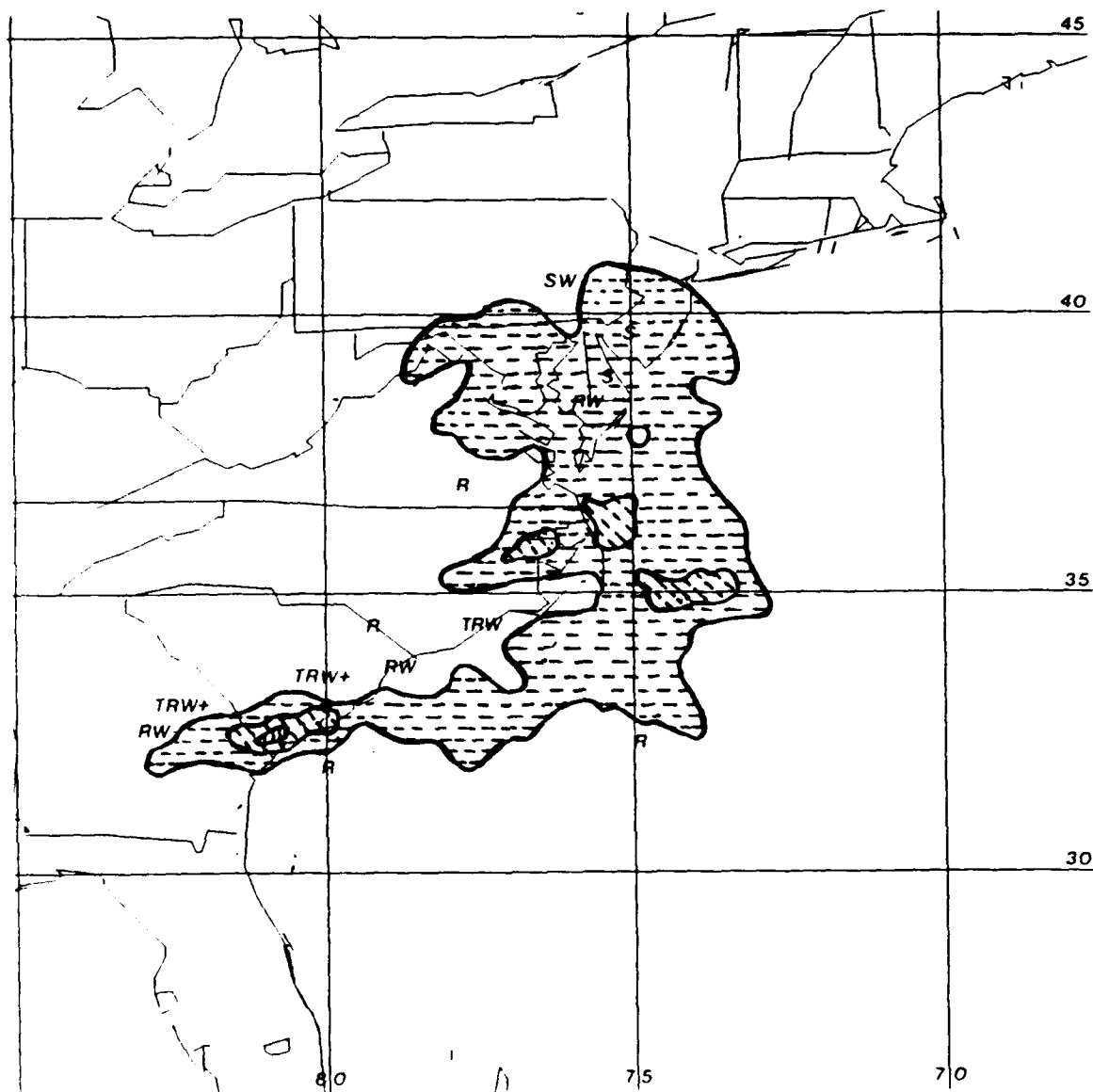
Fig. 16 3/2335 January 1989 Radar Summary Chart. [Drawn from 3/2335 January 1989 ARS chart]

on both the SSM/I analysis and radar summary. The small area of no precipitation off the coast of South Carolina and North Carolina is correctly analyzed.

Contour levels indicate the majority of the precipitation is less than 13 mm/h. Several cells are depicted as having rainfall rates greater than 13 mm/h. The cell

37

at 35N 73.5W with maximum rainfall rates of 9-10 mm/h matches the cell on the ARS chart that displays a level 3 intensity. The elongated cell at 36N 73W with intensities of 7-8 mm/h is near another ARS cell depicted as level 3. The exponential algorithm is underestimating the intensities in these two cells but the algorithm is able to identify those regions where the rainfall rates are higher than the surrounding precipitation areas. An ARS level 5 contour can be seen over southeastern Georgia showing intense convective activity with rainfall rates as high as 180 mm/h. The strong cell of thundershowers over southeastern Georgia cannot be verified since the exponential algorithm is for oceanic precipitation. An SSM/I land algorithm would be needed to analyze this area. The precipitation analysis did not reveal the snow showers present on the radar summary north of 38N due to the SSM/I being less sensitive to snow versus liquid water.

c. *SSM/I Data for 12/2303 December 1988*

Fig. 17 presents the exponential algorithm precipitation analysis for the 12/2304 December 1988 SSM/I pass. A large, irregular-shaped area of precipitation is analyzed off the South Carolina-Georgia coast extending out to 71W. The region is associated with the first cyclone center of IOP 2. The northern tip of this area reaches to 34N. A line of isolated cells stretches from 28N 67W to the southern tip of Florida. A one degree band of missing data is located near 27N from one edge of the pass to the other. The band of missing data cuts across the lower portion of the main body of precipitation. The large area of precipitation shows maximum intensities of 5-6 mm/h

38

near the center. Cells near southern Florida and Cuba shows maximum rainfall rates of 9-10 mm/h.

d. Radar Summary Charts for 12/2135 and 13/0135 December 1988

The ARS charts closest to the 12/2303 SSM/I pass were not available, but the 12/2135 and 13/0135 radar summary charts (Figs. 18 and 19) that bracket the time of the pass will be used for comparison. The 12/2135 radar summary shows a hook-shaped area over Georgia and along the South Carolina-North Carolina coast. The rainfall rates in this area are less than 13 mm/h. A smaller area of rain and rain showers is located off the eastern coast of Florida. An isolated cell near the center of this area indicate intensities of level 3. These two areas appear to have merged on the 13/0135 radar summary charts. A long region of precipitation stretches from North Carolina down to Florida. Most of the precipitation is rain with snow found near the coast in the northern part of the region. The rainfall rates throughout this stretch are less than 13 mm/h.

The SSM/I rain analysis off the coast of South Carolina and North Carolina correlates well with the two radar summary charts. Intensities of 1 to 6 mm/h are reasonable compared to the rainfall rates recorded on the radar summary charts. The precipitation analysis does not extend into South Carolina and North Carolina, but surface observations at 12/2300 indicate snow and snow showers along the Carolina coast. No SSM/I precipitation analyzed suggest this area may have snow or snow showers in the vicinity as reported on the ARS charts.

Cells near the southern tip of Florida are reported on both radar summary charts. The 12/2135 radar summary shows a single cell that has contour level of 3

39

Fig. 17   12/2...4 December 1988 Exponential Algorithm Rainfall Rate Analysis
Longitude line is 70W

indicating rainfall rates at the center range above 14 mm/h.   On the 1801 W radar
summary, two cells are reported in the same area.   These two cells also have contents
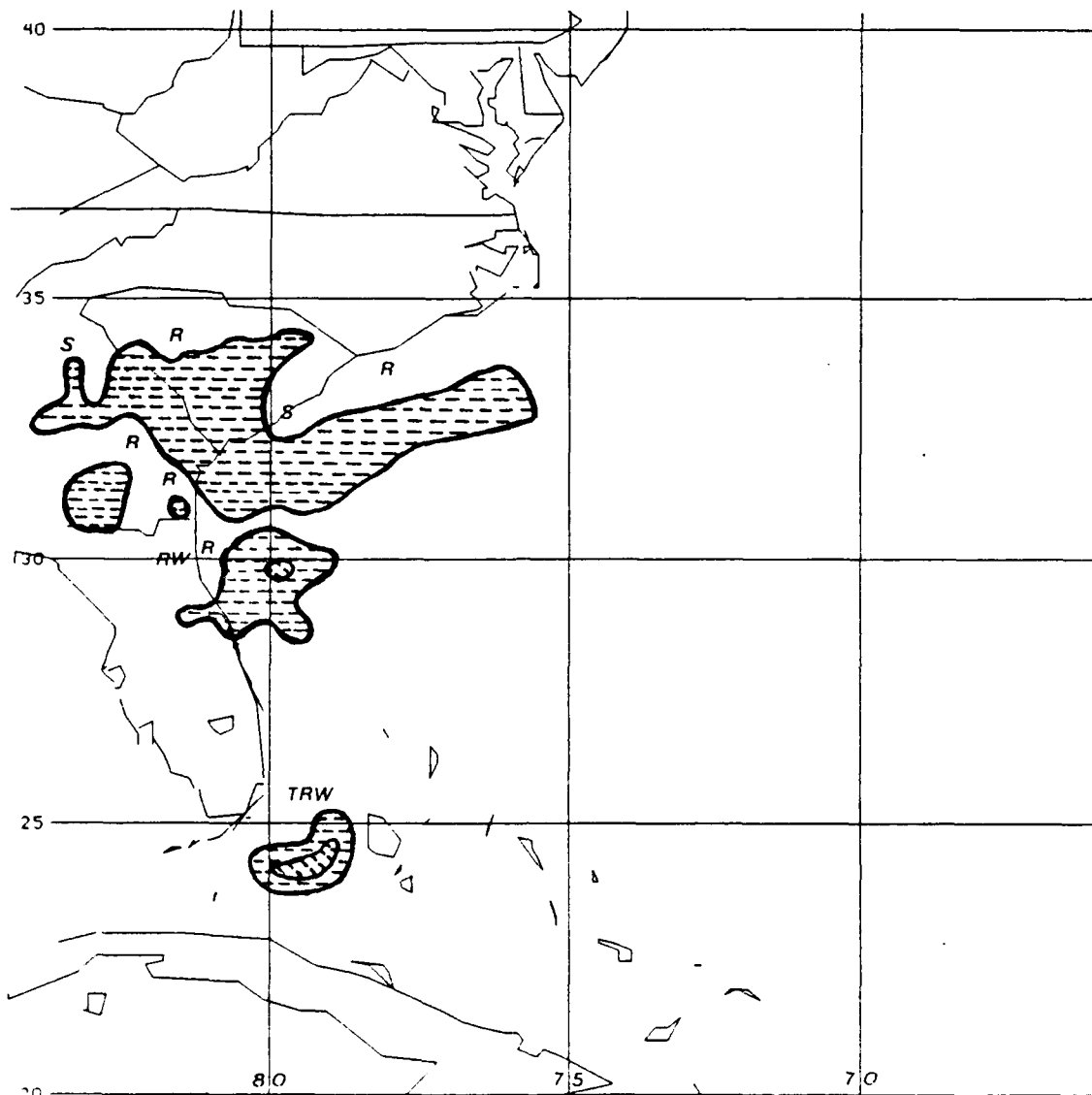
Fig. 18 12/2135 December 1988 Radar Summary Chart. [Drawn from 12/2135 December 1988 ARS chart.]

level 3 near the center. The 12/2303 SSM/I rain analysis analyzes these convective cells in this area. The maximum intensities analyzed in these cells are slightly lower, but the analysis is able to detect the higher rainfall rates.

41
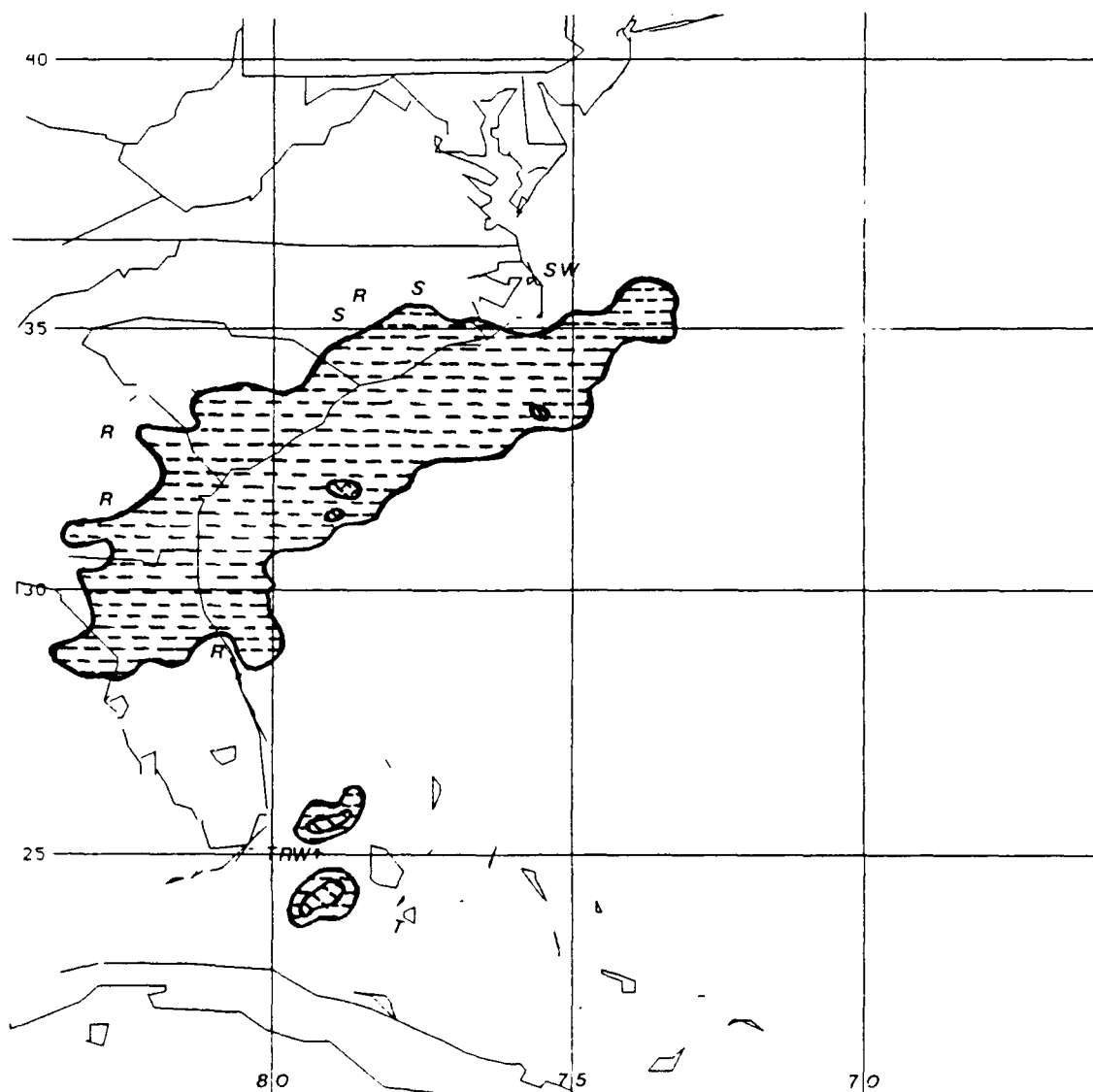
Fig. 19 13/0135 December 1988 Radar Summary Chart. [Drawn from 13/0135 December 1988 ARS chart.]

e.   Comparison Summary.

The SSM/I rain analyses showed general agreement with the radar rain coverage found on corresponding radar summary charts. Outer boundaries of rain areas contoured by the charts are well described by the exponential algorithm. Maximum rainfall rate areas also coincide well with the higher contour levels of precipitation

42

activity. The rain intensities in the SSM/I maximum rain regions tend to be less than those found in the radar summary charts. Areas in the radar summary charts showing light snow or snow showers are not detected by the microwave data.

Two additional SSM/I rain analyses in IOP 2, 13/0904 and 13/2258 December 1988 (not shown), were also compared with radar summary charts. The 13/0904 SSM/I rain analysis observed the rain pattern of the first developing cyclone center. The cyclone's main precipitation area is too far for coastal radar coverage, but a narrow band of light rain was located approximately one degree longitude from the North Carolina coast. The corresponding radar summary chart verified the presence of this rain band.

The second cyclone center that developed in IOP 2 is the major rain feature on the 13/2258 SSM/I rain analysis. Again, the primary rain area occurs in the comma head region, but is beyond radar coverage. However, a rain band north of the comma head region extends toward the Connecticut-Massachusetts coast. This rain area correlates well with the radar summary chart except north of 42N where snow was observed. The SSM/I and radar rain intensities were also comparable. The main difference in the two additional cases was the SSM/I precipitation extent covered a smaller area than depicted on the radar summary charts.

IV. SSM/I RAIN ANALYSIS - IR SATELLITE IMAGERY COMPARISON

Extensive research has been completed estimating precipitation using IR and visible satellite data. Although IR and visible satellite techniques are indirect methods, i.e., the raindrops themselves are not directly sensed by IR or visible radiation, studies show there is a relationship between rainfall rates and cloud brightness and its cloud top temperature. Lovejoy and Austin (1979) used brightness and temperature observations from IR and visible data together to estimate precipitation in conjunction with weather radar data. They found clouds with very cold tops produced the heaviest precipitation. Adler and Negri (1988) developed a scheme, the Convective-Stratiform Technique (CST), by using only infrared satellite data to estimate rainfall rate. In their satellite analysis, they located minima in the IR temperatures that are assumed to be convective elements. By determining the cloud top temperatures at these minima, rain areas and rainfall rates can be assigned to the convective elements. This chapter will compare SSM/I rain analyses with corresponding enhanced IR satellite data to illustrate the evolution of rain patterns in oceanic rapid cyclones and their relation to cloud IR patterns.

A. GOES INFRARED DATA

The Geostationary Operational Environmental Satellite (GOES) system produces one-half hour IR satellite imagery. The GOES digital IR imagery have 8-bit radiometric resolution (Clark et al 1983). To identify the significant cloud features, the contrast

44

between those features and their background must be increased. This is accomplished by using enhancement curves.

Numerous enhancement curves have been tested by the Satellite Services Division of the National Environmental Satellite, Data, and Information Service (NESDIS). The enhancement curve developed for estimating precipitation is the MB curve. Fig. 20 shows a graph of the MB curve indicating several important ranges of temperatures with their associated gray shades. Description of the key temperature ranges are found in Table 2. Segments 4 through 7 are used to analyze convective activity. The IR satellite imagery compared with the SSM/I rain analyses are enhanced with the MB curve.

B.   SSM/I - GOES COMPARISON FOR IOPS 2 AND 4 CYCLONES

Two series of three SSM/I rain analyses from IOP 2 and 4 will be compared with related GOES IR satellite imagery. The 12/2304, 13/0904, and 13/2258 December 1988 SSM/I passes from IOP 2 and the 3/2333, 4/0932, and 4/2147 January 1989 passes from IOP 4 will provide the rain analyses.

1.   IOP 2 CYCLONE

The IOP 2 cyclone started as multiple low centers on 13 December 1988. The first surface low developed shortly after 13/0000 when the first of two upper-air troughs moved offshore along the Georgia-South Carolina coast. This initial surface low deepened modestly for the initial 12 h period. A second and stronger upper-air short wave trough, with an associated upper-level jet streak, moved offshore from Virginia and North Carolina about 13/1200 and triggered a second surface low northwest of the first

45

COUNT VALUE (INPUT)

```
        000        051        102        153        204        255
WHITE
                                                              9
204

GREY SCALE                                          5
                                                              COUNT VALUE (OUTPUT)
                                        3           153
                                                          8
                                                    102
                                            4
              2
                                                6   051
                                                        
BLACK    1                                    7   000
```

```
        134        88.4       42.5       -3.4      -74.5      -165 °F
        56.8       31.3       5.8       -19.7      -59.2      -109 °C
        330        305        279        253        214        164 °K
```

TEMPERATURE
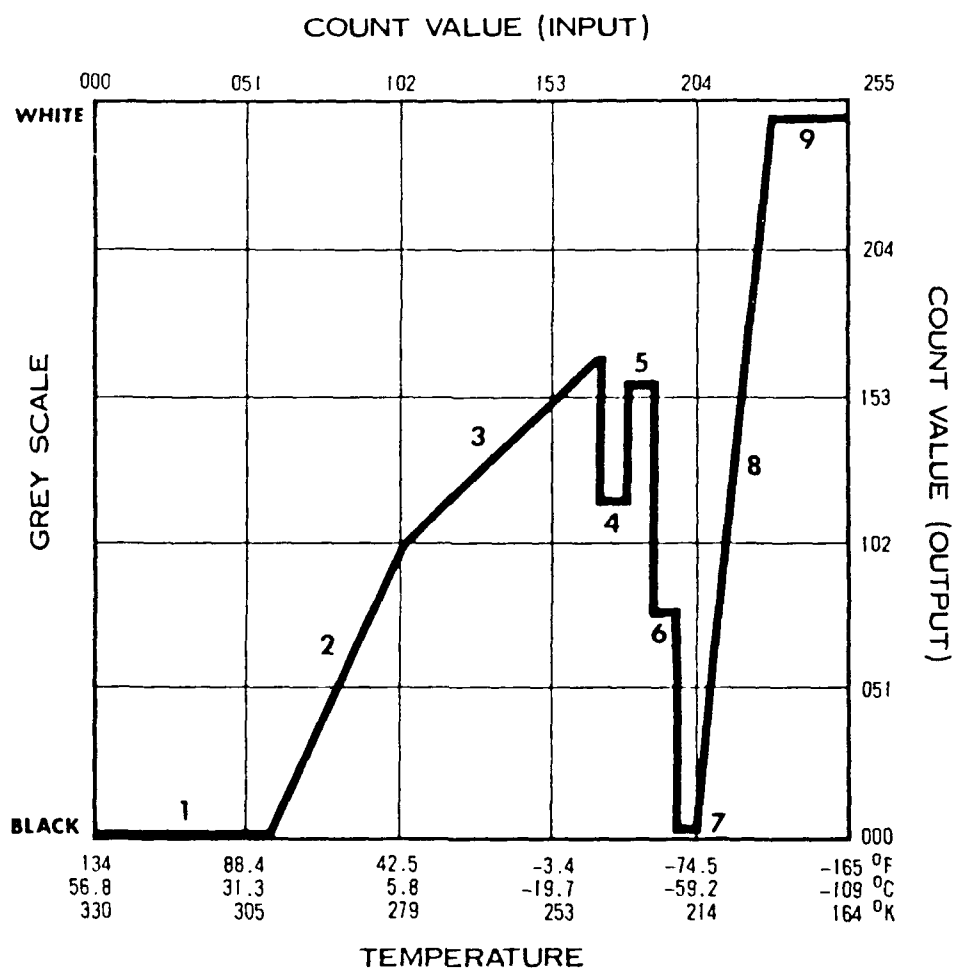
Fig. 20 Graphical display of MB Enhancement Curve. [After Clark et al 1983]

surface low. Between 14/0300 and 14/0900, the cyclone central pressures fell by 18mb/6h (Hartnet and Hadlock 1989).
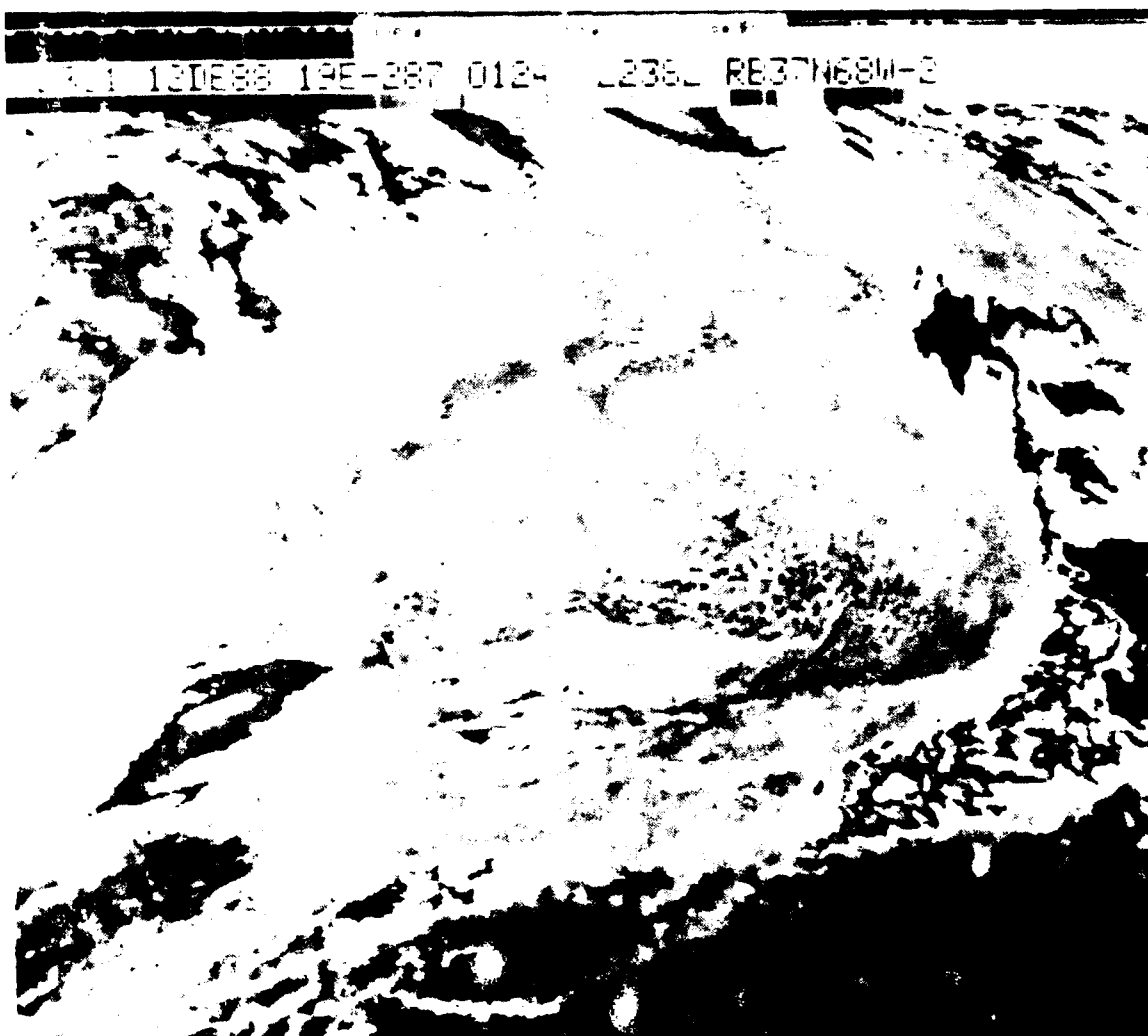
a. 12/2304 December 1988

The initial cyclone that started to develop offshore of South Carolina had a central pressure of approximately 1010 mb. On the 12/2301 GOES IR imagery (Fig. 21), a large region of low to middle level clouds extends over the North Atlantic Ocean with an old frontal system on the eastern edge of the image. Near the Georgia and South

46

Table 2 DESCRIPTION OF MB ENHANCEMENT CURVE. [After Clark et al 1983]

SEGMENT NUMBER	°C TEMPERATURE	COMMENTS
1	58.8 to 29.3	Little or no useful data (Black)
2	28.8 to 6.8	Low Level/Sea Surface Difference
3	6.3 to -31.2	Middle level - No Enhancement
4	-32.2 to -42.2	First Level Contour (Medium Gray)
5	-43.2 to -53.2	Second Level Contour (Light Gray)
6	-54.2 to -59.2	Thunderstorm Enhancement (Dark Gray)
7	-60.2 to -63.2	Thunderstorm Enhancement (Black)
8	-64.2 to -80.2	Overshooting Tops Enhancement (White)
9	-81.2 to -110.2	Overshooting Tops Enhancement (White)

Carolina coast is an area of higher level clouds associated with the incipient cyclone. An elongated zone of enhanced cold cloud tops (colder than -32.2°C) parallels the coastline from northern Florida to the southern part of North Carolina. The coldest cloud top temperatures (-43.2 to -53.2 °C) are centered in this zone about 32.5N 79W. A second narrow band of cold cloud tops is located east of southern Florida. Coldest temperatures in this band range are colder than -65°C indicating thunderstorm activity.

The 12/2304 December 1988 SSM/I rain analysis (See Fig. 17, Chapter III) shows a broader area of precipitation off the coast of South Carolina. The algorithm that includes one usable 85 GHz channel (Equation 7) is used on this and all subsequent rain rate analyses. The 19 and 37 GHz only algorithm (Equation 6) matches the other approach, but cannot resolve the intensity of the rain rate maxima. A large cell with maximum rainfall rates of 5-6 mm/h is centered near 31N 78.5W, near the coldest IR

Fig. 21 12/2301 December 1988 GOES Enhanced IR Imagery.

cloud tops. Two smaller cells with maximum rain intensity of 5-6 mm/h are also analyzed in this broad precipitation area. The outbreak of this precipitation is correlated with the start of development of this cyclone. The SSM/I rain rate analysis also shows a broken line of precipitation cells east of Florida. This line has maximum rainfall rates of 11-12 mm/h that correlates well with the narrow band of cold cloud temperatures described in the IR imagery.

b. 13/0904 December 1988

The second SSM/I pass in IOP 2 occurred 10 h later. The cyclone had developed into a comma-shaped cloud system as shown in the 13/0901 December GOES IR imagery (Fig. 22). The central pressure of the cyclone had decreased to approximately 1004 mb (6mb/10h). The comma head is large and ragged with the coldest cloud tops contoured in an anvil shape near the center. The comma tail is not well organized with isolated, cold, embedded cells. The coldest temperatures in the comma head and tail range from -60.2 to -63.2°C.

The SSM/I rain analysis for 13/0904 December 1988 (Fig. 23) shows a comparable comma shape. A large precipitation comma follows the enhanced IR imagery. Maximum rainfall rates have increased to over 12 mm/h near the center of the comma head. This agrees well with the IR imagery and cloud top temperatures of less than -60°C. In the comma tail (approximately 28.5N 71W), an area of maximum rainfall rates greater than 12 mm/h (highest rain rate detected is 21 mm/h) coincides with additional enhanced IR cells. The realistic synoptic structure of the SSM/I rain analysis and its strong correlation to the IR cloud top patterns are further evidence of the success of this rain rate algorithm.

c. 13/2258 December 1988

The next comparison period showed the first surface low continuing to move to the east, while a much deeper low was developing east of North Carolina and Virginia. The central pressure of the second cyclone at 13/2300 was approximately 995 mb. In the 13/2231 December 1988 IR imagery (Fig. 24), the cyclone near the coast is

49
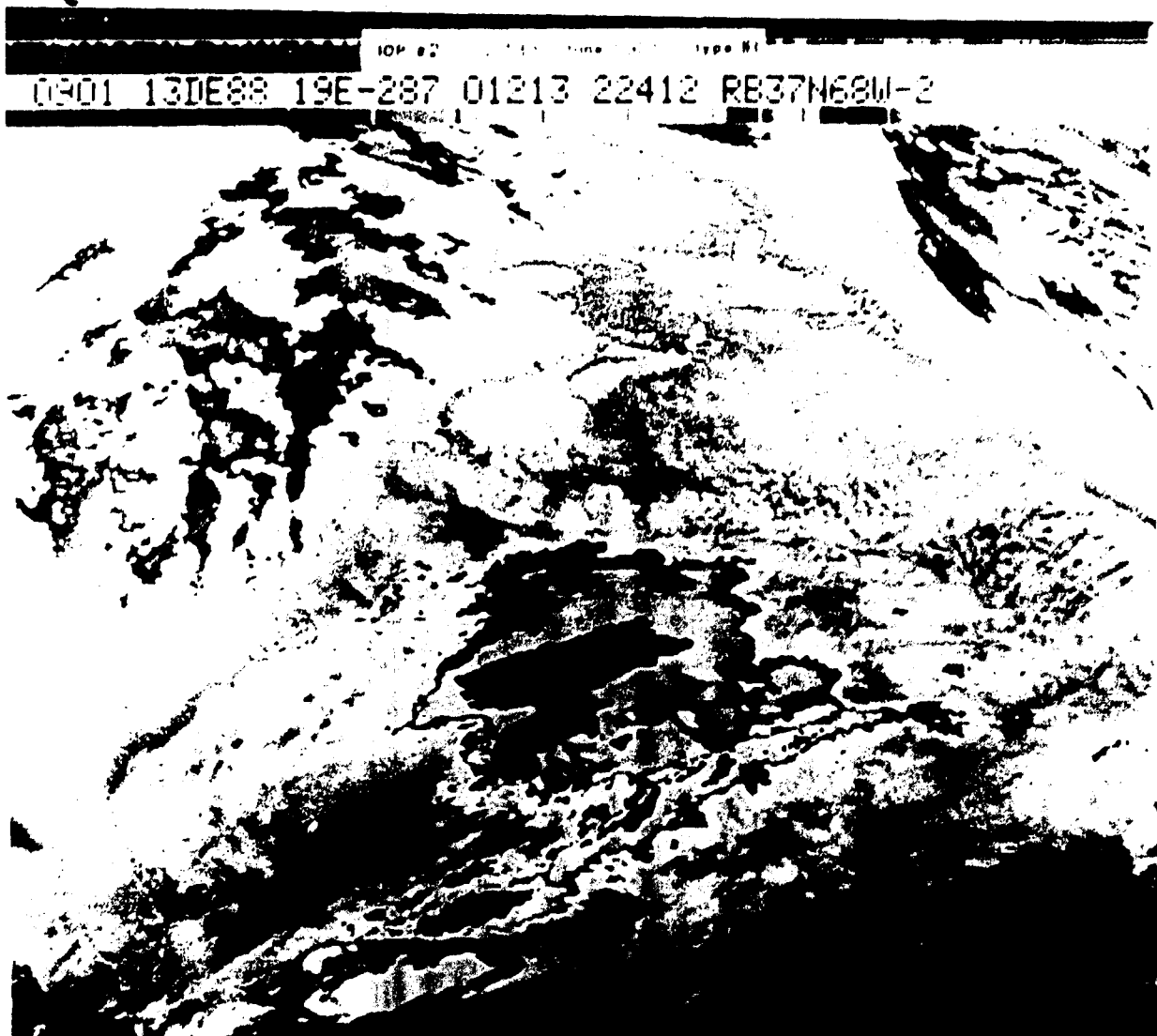
Fig. 22 13/0901 December 1988 GOES Enhanced IR Imagery.

depicted as an oval-shaped area. Enhanced IR data areas extend from 43N to 33N and from 73W to 67W and inland to the northwest. The coldest temperatures range from -43.2 to -53.2°C.

The 13/2258 December 1988 SSM/I rain analysis (Fig. 25) captures rain with the western part of the first cyclone and the developing second cyclone. The second cyclone precipitation correlates well with the large shield of cold cloud tops in the IR imagery. The center of the rain area is located at approximately 37N 71W with

Fig. 23 13/0844 December 1988 Exponential Algorithm Rainfall Rate Analysis. Latitude and longitude lines are 10° apart. Southern latitude is 30N and western longitude is 80W.
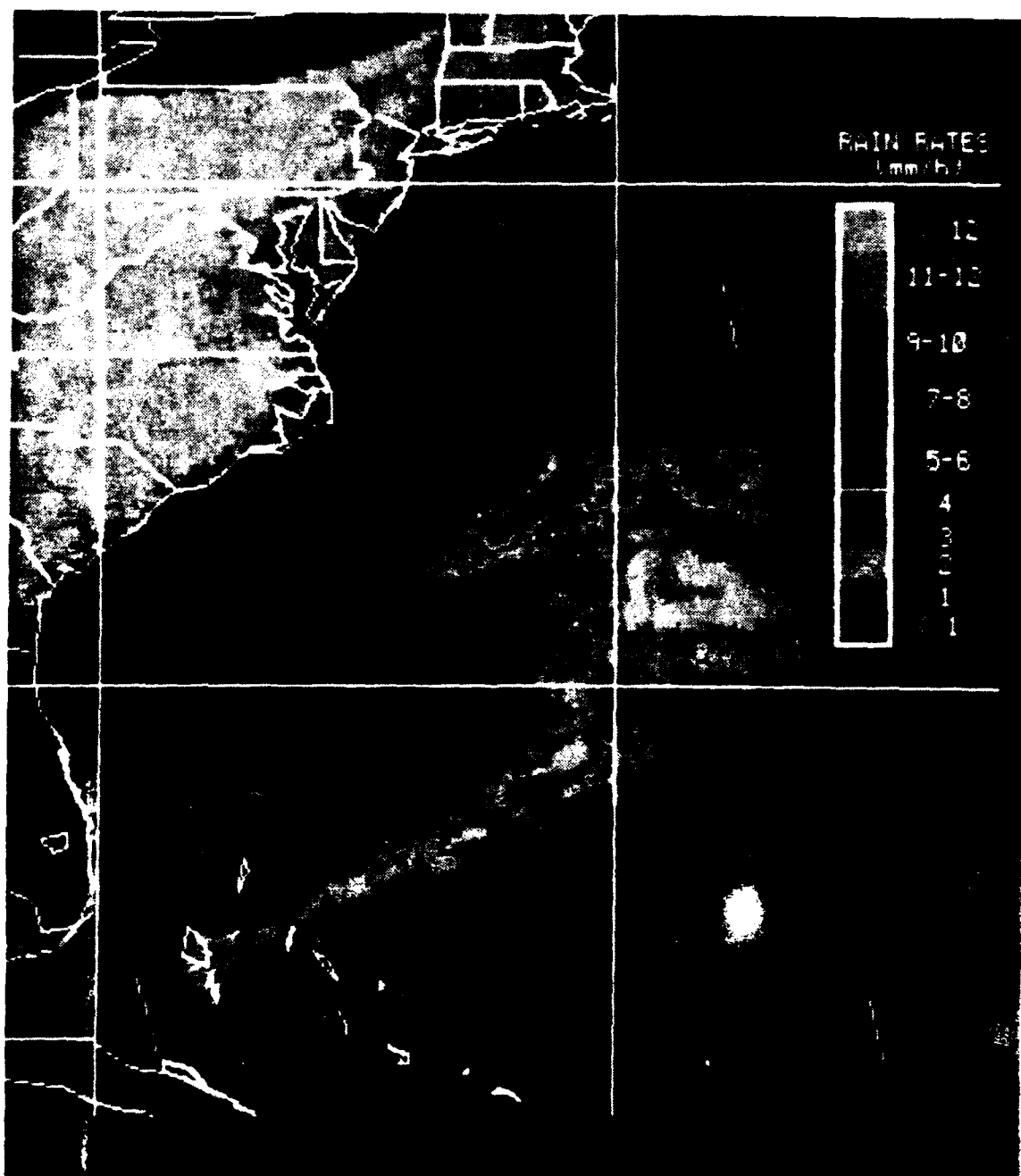
51
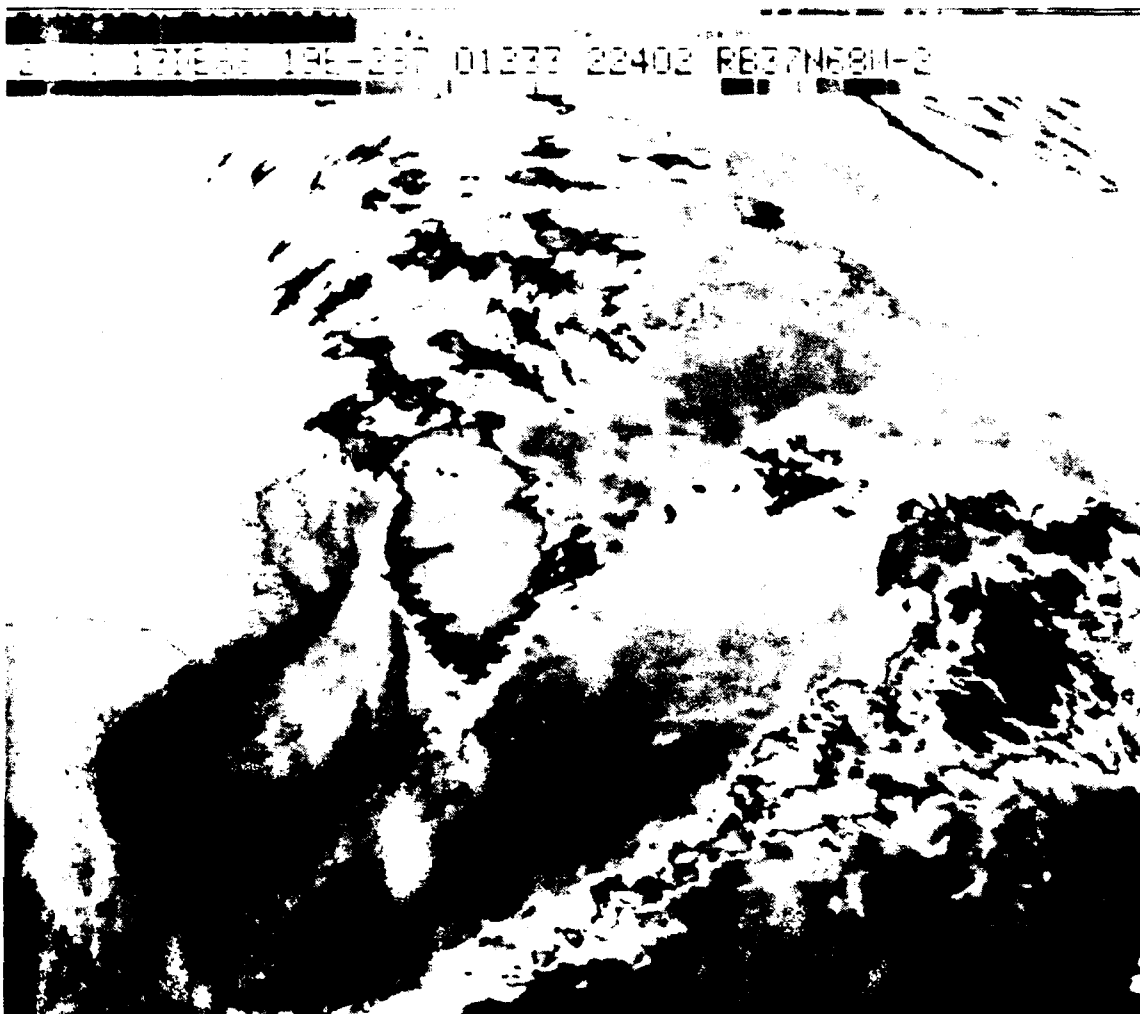
Fig. 24 13/2231 December 1988 GOES Enhanced IR Imagery.

maximum rainfall rate greater than 12 mm/h (highest rain rate is 21 mm/h). The

enhanced IR does not indicate colder cloud tops with these embedded, high rainfall rates.

The extension to the northwest contains a zone with SSM/I rainfall rates of 0-10 mm/h.

The IR cloud top temperatures in this area range from -32.2 to -42.2°C. Light

precipitation is analyzed by the SSM/I west of the first low in an area of warmer cloud

tops. The rapid development of the intense SSM/I precipitation confirms strong vertical

motions and convection are present in the second cyclone. This system deepened 30 mb in the next 12 hours. Unfortunately, SSM/I data is not available at that time.

2.   IOP 4 CYCLONE

The IOP 4 cyclone may have been the deepest extratropical cyclone to occur south of 40N in this century (Hartnet and Hadlock 1989). Its central pressure fell to 938 mb on 5/0300 January 1989 with an estimated deepening rate of 24 mb/6h occurring between 4/0900 and 4/1500. The cyclone appeared to take the form of a trough containing several low centers as it developed off the coast of North Carolina. When a strong, upper-air disturbance reached the coastline about 4/0000, the cyclone rapidly deepened and became a powerful, single center cyclone.

a.   3/2333 January 1989

At this time, the cyclone started to develop off the Carolina coast prior to its rapid intensification. Its central pressure was approximately 995 mb. The 3/2301 GOES IR imagery (Fig. 26) shows a broad, elongated area of middle to high clouds, associated with the incipient cyclone, located off the coast of South and North Carolina. Enhanced cold cloud tops (colder than -32.2°C) extend from 32N to 36N and from 75W to 63W. A smaller area of cold cloud temperatures is located northwest of this large convective region near 37N 74W. An earlier storm, that also deepened rapidly, is located northeast of the IOP 4 cyclone.

The 3/2333 January 1989 SSM/I rain analysis (See Fig. 15, Chapter III) shows an irregular-shaped area of precipitation. The main precipitation area is over water
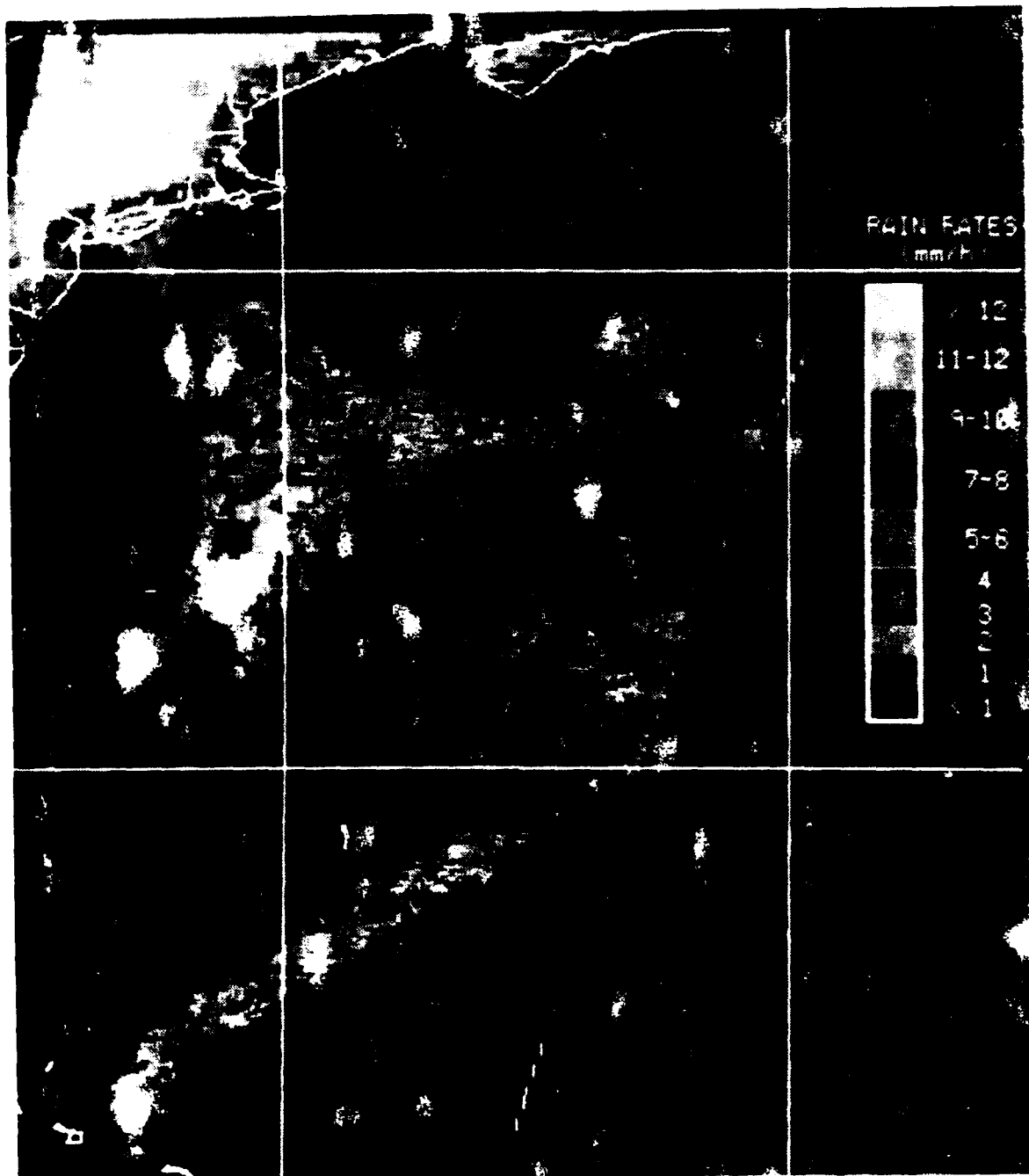
53

Fig. 25   13/225s December 1985 Exponential Algorithm Rainfall Rate Analysis. Latitude and longitude lines are 1° apart. Southern latitude is 30N and western longitude is 70W.
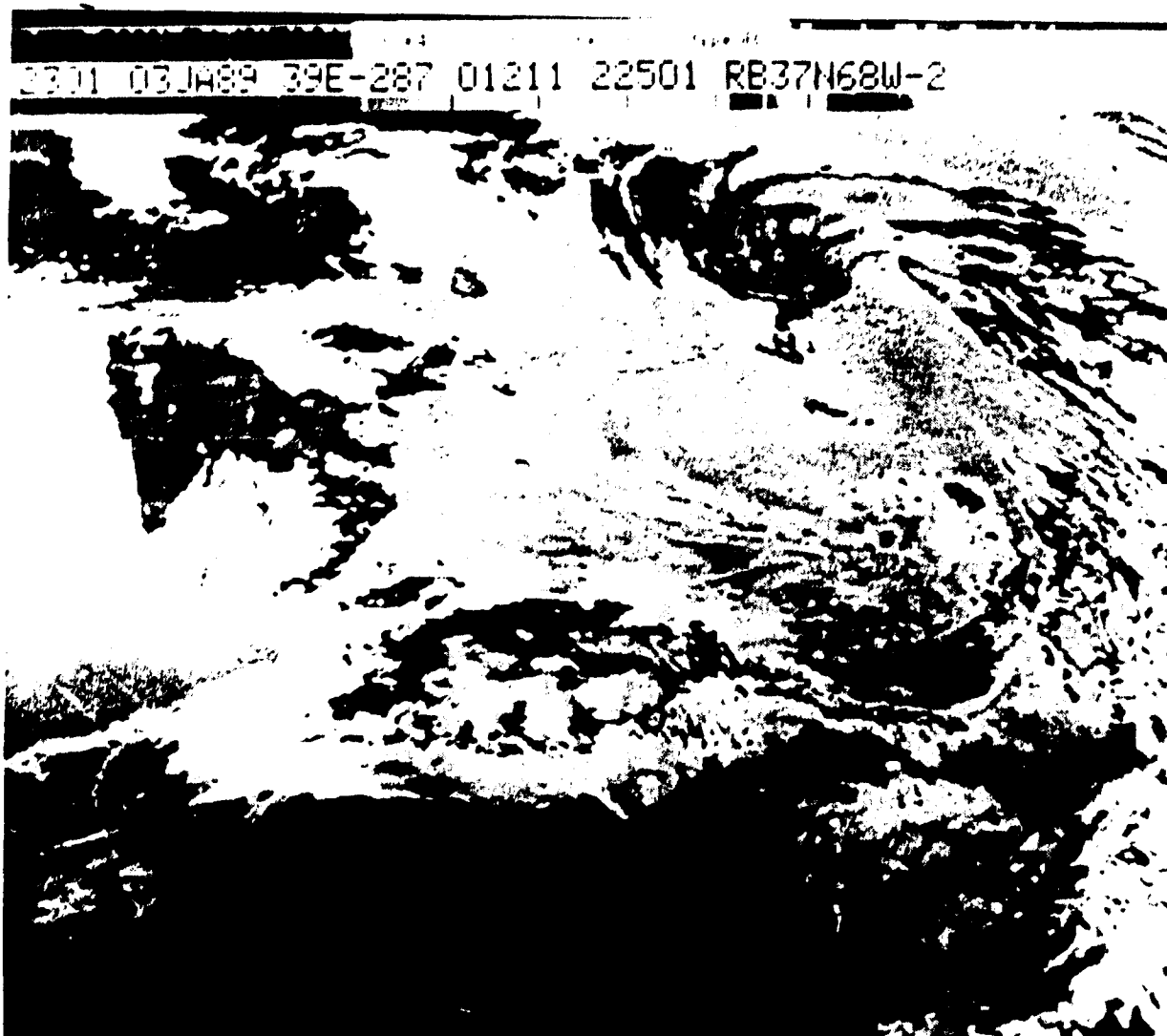
Fig. 26 3/2301 January 1989 GOES Enhanced IR Imagery.

except near the North Carolina coast. The western edge of the SSM/I rain area is closer to the coastline than the convective area in the IR imagery. Four distinct cells with maximum rain rates of 9-10 mm/h are resolved in the SSM/I rain region. The northern cell coincides with the smaller IR rain area near 37N 74W. The other three rain cells are not distinguishable in the IR imagery. The SSM/I rain rate data indicates significant precipitation in the early development stages of this cyclone like IOP 2.

b. 4/0932 January 1989

Over the next 12h, the cyclone rapidly deepened and developed into a well-defined comma cloud system. Central pressure dropped to approximately 970 mb, a 25 mb decrease in 10 hours. The 4/0931 GOES imagery (Fig. 27) shows the comma-shaped cloud system with an extensive canopy of enhanced cold cloud tops stretching eastward to about 52W. Slightly southeast of the comma head (39N 64W) are two small areas of very cold cloud tops (-59.2 to -62.2°C) indicating heavy thunderstorms. The northernmost edge of the enhanced, cold cloud top is located at 46N. The comma tail extends southward towards southern Florida with very isolated thunderstorms cells.

The 4/0932 January 1989 SSM/I rain analysis (Fig. 28) only captures the eastern half of the cyclone due to the limited swath width of the SSM/I instrument. There is no data available over the western section of the storm since the SSM/I passes are not contiguous. Rain extends from the comma head to approximately 55W. Three cells of high rainfall rates are analyzed with maximum rain rates of greater than 12 mm/h (highest rain rate detected is 20 mm/h). The cell at 38N 65W and the cell to the south correlate well with the two areas of coldest cloud tops in the IR imagery. The eastern cell analyzed by the exponential algorithm is not discernable in the IR imagery. The northern edge of the cyclone precipitation (40N) does not extend as far north as the enhanced IR similar to the IOP 5 case. Coastal reports indicate snow in this northern sector.

c. 4/2147 January 1989

The continued development of the cyclone is indicated by the GOES 4/2201 January 1989 imagery (Fig. 29). The comma structure of the cyclone increased
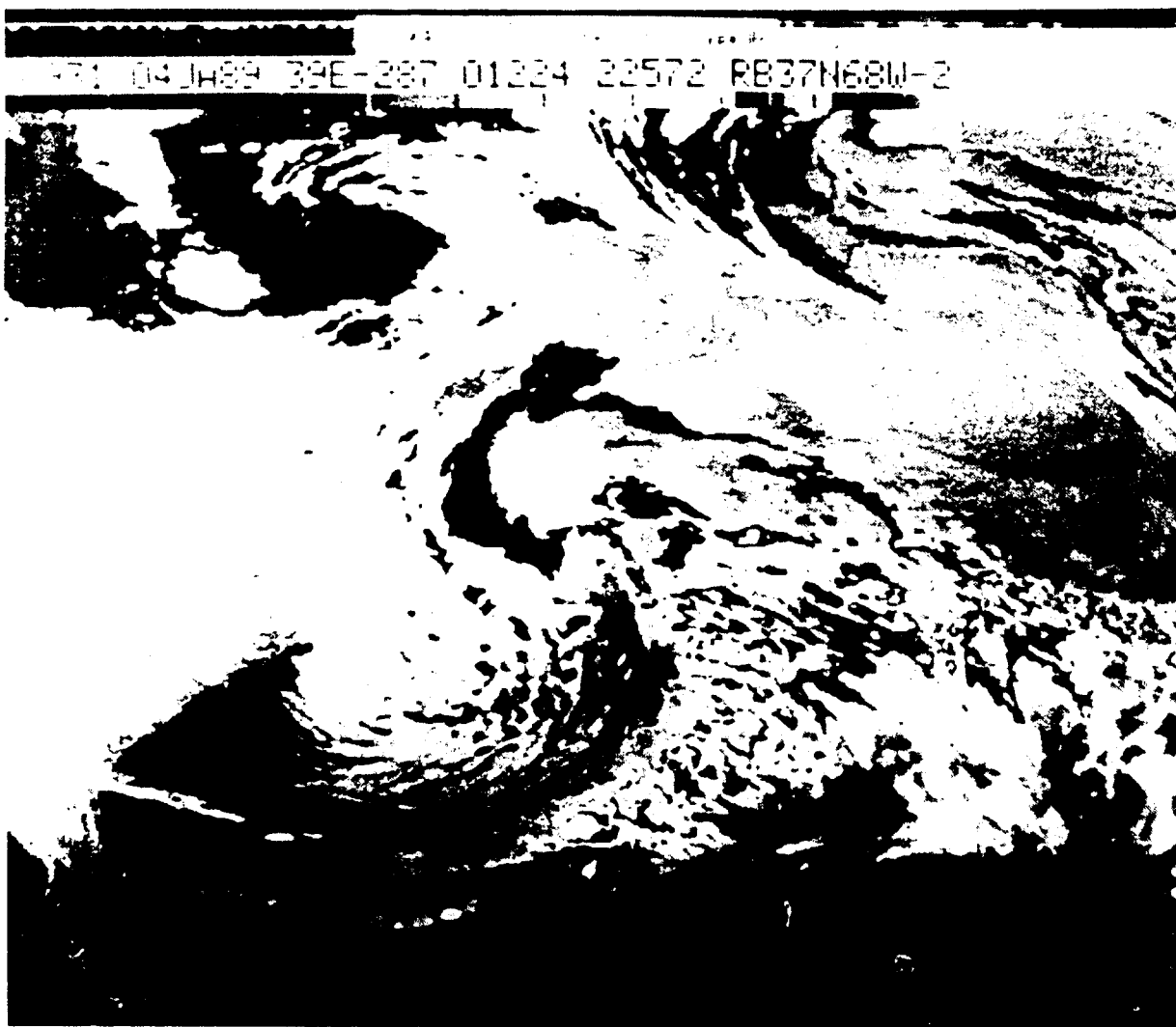
Fig. 27 4/0931 January 1989 GOES Enhanced IR Imagery.

in size and strong northwesterly flow of cold air to the rear of the storm was evident. The central pressure was 948 mb, a drop of 22 mb in 13 hours.

The IR cloud imagery shows the comma head wrapping around the low center positioned at 39N 59W. The northernmost edge of the convection is near 49N. The coldest cloud tops (less than -60°C) are found mostly along the comma tail where scattered thunderstorms are embedded. A small area of very cold cloud tops (-60 to -63°C) near 44N 52W is located east of the comma head.
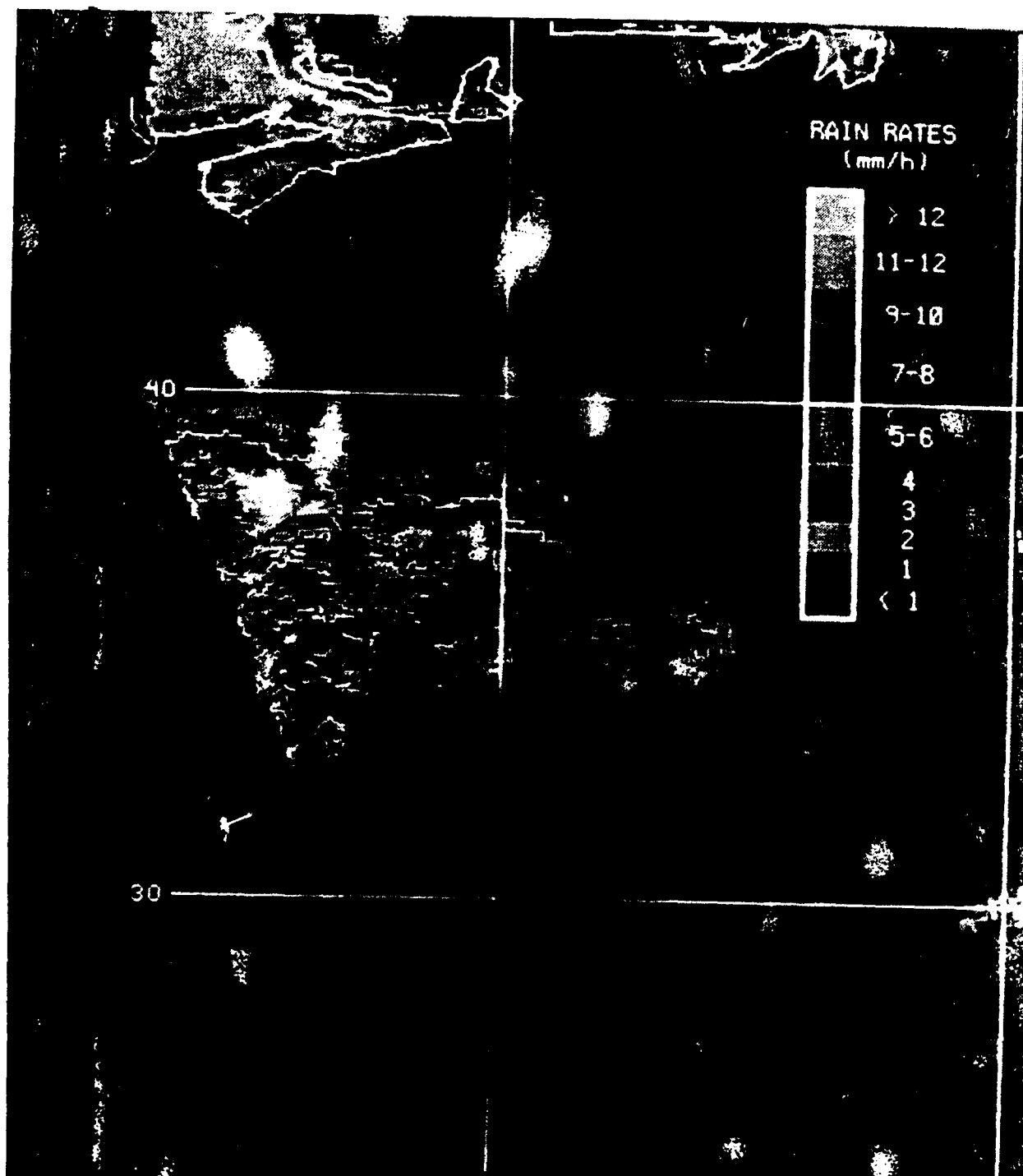
57

Fig. 28 4/0 ₂2 January 1989 Exponential Algorithm Rainfall Rate Analysis. Longitude
lines are 10° apart. Western longitude is 60W.

The 4/214ᵇ January 1989 SSM/I rain analysis (Fig 30) depicts the eastern

half of the cyclone The comma tail is the predominant feature analyzed Several cells

58
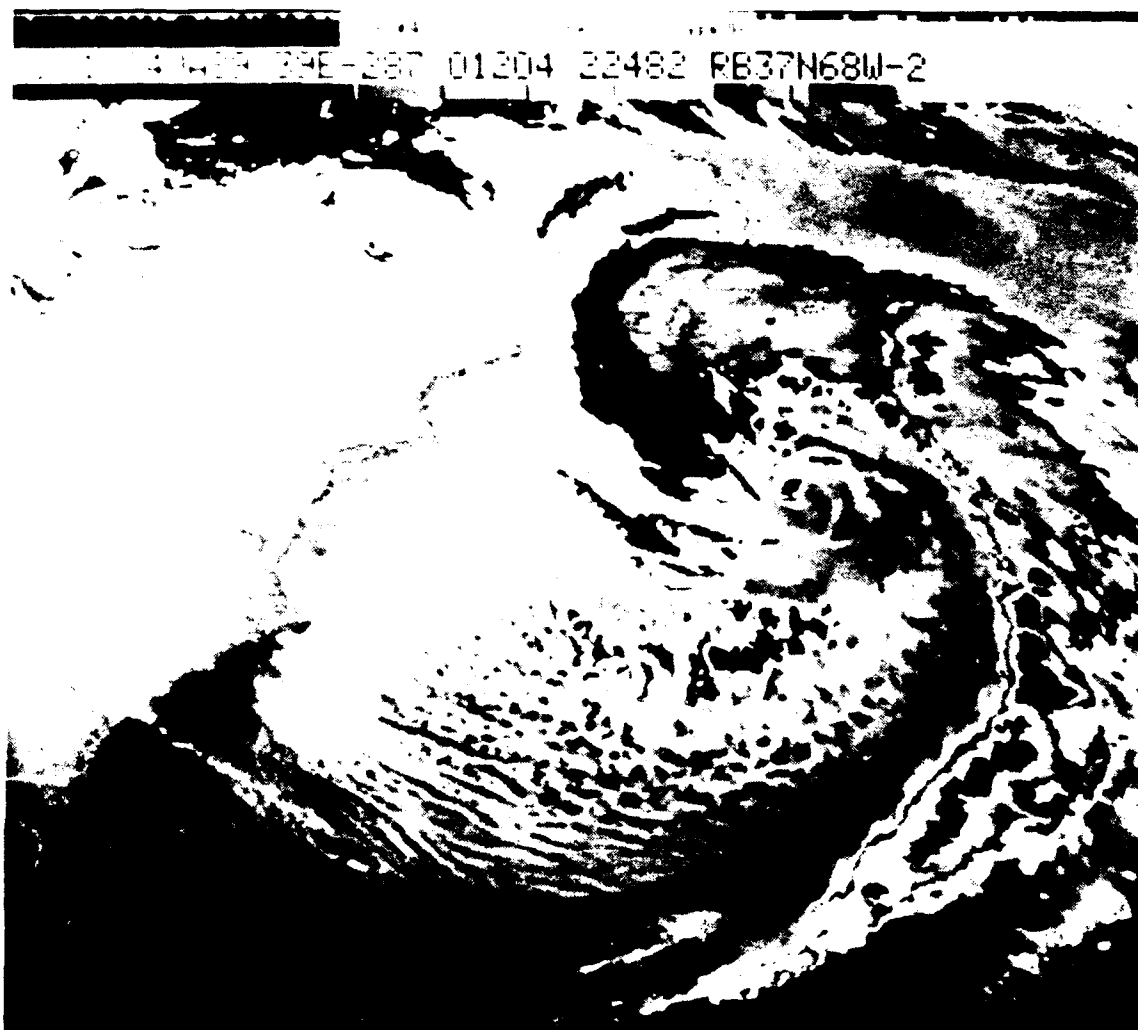
Fig. 29 4/2201 January 1989 GOES Enhanced IR Imagery.

along the tail indicate high rain rates with maximum rainfall rates greater than 12 mm/h

(highest rain rate detected is 20 mm/h). The analyzed cell near 41N 52W nearly coincide

with the very cold cloud top area (44N 52W) in the IR imagery. Another high SSM/I

rain rate area centered at 44N 56W is not distinguishable on the IR imagery. A gap in

the IR convective clouds slightly west of the cold cloud top area (44N 52W) is also

depicted in the SSM/I rain analysis. An analyzed band of rain paralleling the comma tail

is not clearly shown on the enhanced IR since this area is very close to the edge of the
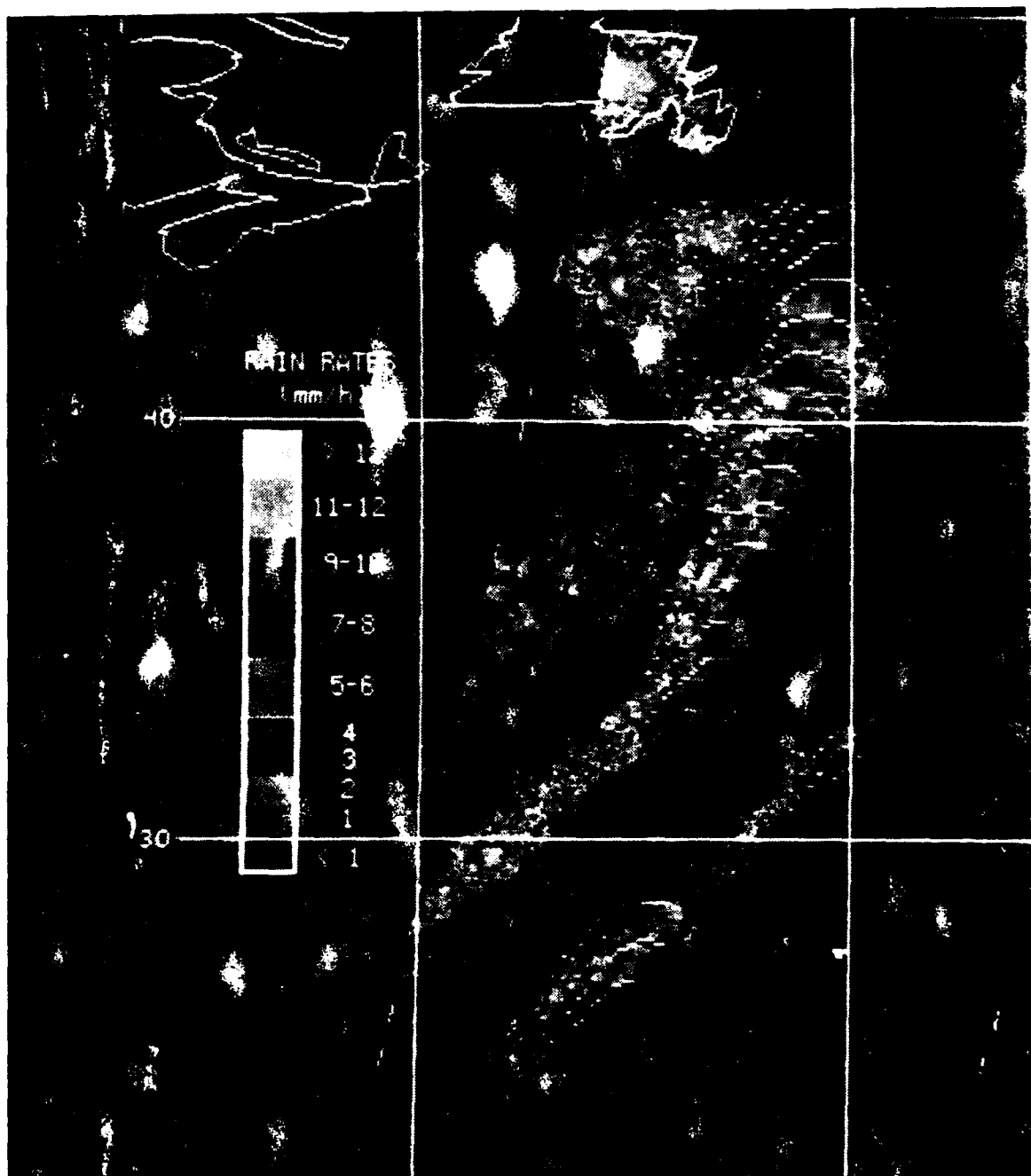
Fig. 30 4 2147 January 1989 Exponential Algorithm Rainfall Rate Analysis Longitude line are 10 apart Western longitude is 60W

IR image.

The sequence of the SSM/I rain analyses in IOP 4 again demonstrates the synoptic signatures of cyclones enhanced in IR imagery can be analyzed by the SSM/I rain analyses. The best evidence of this is the well-defined comma tail depicted on the 4/2201 January 1989 IR image that was captured extremely well by the 4/2147 SSM/I rain analysis.

A third series of SSM/I rain analyses from IOP 3 (not shown) were also compared with enhanced IR imagery to further study cyclone development. However, it was impossible to complete the comparison since the SSM/I passes generally did not capture the rain areas of the cyclone. The cyclone was located in the "missing data" area between SSM/I passes at the key analysis times. Cataldo (1990) did discuss IOP 3 passes as they covered the edges of the cyclone.

V. SUMMARY AND CONCLUSIONS

The measurement of microwave radiances provides a direct estimate of rain rate. The SSM/I on the DMSP satellite provides operational microwave data. This thesis studied a recently developed SSM/I exponential rain algorithm that used the nonlinear relationship of rain rate and the rain's brightness temperature. SSM/I microwave data from several ERICA cyclones in IOPs 2, 3, 4, and 5 were analyzed by the exponential rain algorithm. Aircraft radar (IOP 5) and coastal radar (IOPs 2 and 4) data were used to validate the SSM/I estimated rain analyses produced by the algorithm that included the usable 85H GHz channel. The 19 and 37 GHz only algorithm was not used since it did not resolve the intensity of the rain rate maxima. SSM/I rain analyses for IOPs 2, 3, and 4 were compared with corresponding GOES enhanced IR imagery to evaluate further the rain algorithm's capability in describing the synoptic rain structure of the cyclones.

The main purpose of this thesis was to study the SSM/I exponential rain algorithm's ability to detect oceanic rain/no rain areas and rain intensity. The SSM/I rain algorithm produced successful results when the SSM/I rain analyses in IOP 2, 4, and 5 were compared with aircraft and ground-based radar data. The IOP 5 SSM/I rain analysis reasonably depicted the general rain structure and rain rate areas of the cyclone when compared with aircraft radar observations. The rain algorithm performed very well in locating three distinct maximum rain rate areas observed by the radar. The maximum rain intensities analyzed by the algorithm are in general agreement with the radar intensity

observations. However, the SSM/I rain rates are somewhat less than inferred by the radar. The precipitation associated with the IOP 5 cyclone's comma shape and its eastward extension was correctly analyzed. The only disagreement in the aircraft/SSM/I comparison was an area due south of the aircraft. The location of this rain area was not consistently analyzed by the aircraft radar. Further study of the radar observations must be done to explain this discrepancy.

Three SSM/I passes from IOP 2 and one pass from IOP 4 were analyzed and compared with relevant coastal radar summary charts. The SSM/I rain patterns again agreed with the radar summaries. Contours of higher level rain intensity (level 3 and above) correlated with maximum rain rate areas on the SSM/I analyses, but the SSM/I rain rates are also somewhat less than the coastal radar estimates. The SSM/I rain patterns generally agreed with the rain contours on the radar summary charts, but the extent of the SSM/I rain was less. The exponential algorithm also did not analyzed storm areas where snow was reported.

The exponential rain algorithm was applied to several sequential SSM/I passes in IOPs 2, 3, and 4. These SSM/I rain analyses were then compared with their respective GOES enhanced IR imagery. The SSM/I rain analyses were able to describe the synoptic characteristics of each of the cyclones during their development. During the incipient stages of development, the enhanced IR showed a broad, elongated region of convection. The SSM/I rain analyses depicted irregular, disorganized regions of precipitation that correlated with the IR imagery. As the cyclones developed, the expected comma cloud signature appeared on the IR imagery. Very cold cloud tops,

63

signifying heavy convection, were located near the comma head and embedded in the comma tail. The exponential rain algorithm successfully analyzed precipitation patterns with similar appearance. Most of the coldest cloud top regions coincided with the maximum rain rates in the SSM/I rain analyses. Isolated SSM/I rain maxima were analyzed that were not described by the GOES IR imagery.

This study of the SSM/I exponential rain algorithm indicate SSM/I rain rate data can provide another useful method to study coastal and marine weather systems. The notable results that the SSM/I rain analyses produced illustrate the improvements (nonlinear relationship) introduced in the algorithm. However, SSM/I data swaths are not contiguous and important sectors of the cyclone can be missed by the sensor.

For future study, a comparison of SSM/I rain rate analyses of non-rapidly developing cyclones with ERICA cases should be undertaken to study the role of precipitation in rapidly developing cyclone development. Examining in more detail the microwave brightness temperature/IR cloud top temperature relationship would be beneficial since SSM/I data is available only twice a day while the GOES IR imagery is available every thirty minutes. Application of the exponential algorithm on other storms would provide additional verification. The SSM/I rain rate data shows promise to significantly improve analysis of precipitation over the ocean, where conventional data is notably sparse.

LIST OF REFERENCES

Adler, R.F., and A.J. Negri, 1988: A Satellite Infrared Technique to Estimate Tropical Convective and Stratiform Rainfall, *J. Appl. Meteor.*, **27**, 30-51.

Barrett, E.C., and D.W. Martin, 1981: The Use of Satellite Data in Rainfall Monitoring, Academic Press, New York, NY, 340 pp.

Battan, L.J., 1973: Radar Observation in the Atmosphere, University of Chicago Press, Chicago, IL, 324 pp.

Cataldo, E.F., 1990: Evaluation of the SSM/I Rain Analyses for Selective Storms in the ERICA Project. M.S. Thesis, Naval Postgraduate School, Monterey, CA, 83 pp.

Clark, J.D., and others, 1983: The GOES User's Guide, NOAA National Environmental Satellite, Data and Information Service, 156 pp.

Fiore, J.V. Jr., and N.C. Grody, 1990: A Classification Algorithm for Monitoring Snow Cover and Precipitation Using SSM/I Measurements, Fifth Conference on Satellite Meteorology and Oceanography, London, England, 4 pp.

Hadlock, R., and C.W. Kreitzberg, 1988: The Experiment on Rapidly Intensifying Cyclones over the Atlantic (ERICA) Field Study: Objectives and Plans. *Bull. Amer. Meteor. Soc.*, **69**, 1309-1326.

Hartnet, E., and R. Hadlock, 1989: Experiment on Rapid Intensification of Cyclones over the Atlantic (ERICA) Field Phase Summary. Department of Physics and Atmospheric Science, Drexel University, Philadelphia, PA, 300 pp.

Hembree, L. A. Jr., 1987: Meteorological Radar and Its Usage in the Navy, NEPRF Tech. Rep. TR 87-01, Monterey, CA 66 pp.

Hollinger, J., 1989: DMSP Special Sensor Microwave/Imager Calibration/Validation Volume I, Naval Research Laboratory, 153 pp.

----, R. Lo, G. Poe, R. Savage, and J. Pierce, 1987: Special Sensor Microwave/Imager User's Guide, Naval Research Laboratory, 120 pp.

Jones, D.M.A., 1956: Rainfall Drop-Size Distribution and Radar Reflectivity, Res. Rept. No. 6, Urbana Meteor. Lab., Illinois State Water Survey.

65

Katsaros, K.B., I. Bhatti, L.A. McMurdie, and G.W. Petty, 1989: Identification of Atmospheric Fronts over the Ocean with Microwave Measurements of Water Vapor and Rain. *Wea. and Forecasting*, **4**, 449-460.

Kidder, S., and T. Vonder Harr, 1990: Principles of Satellite Meteorology. Academic Press, New York, NY, in printing.

Lovejoy, S., and G.L. Austin, 1979: The Delineation of Rain Areas from Visible and IR Satellite data for GATE and Mid-latitudes, *Atmosphere-Ocean*, **17**, 77-92.

Marshall, J.S., and W.M.K. Palmer, 1948: The Distribution of Rain Drops with Size. *J. Meteor.*, **5**, 165-166.

Olson, W.S., F.J. LaFontaine, W.L. Smith, R.T. Merrill, B.A. Roth, and T.H. Achtor, 1990: Validate Algorithms for the Determination of Rainfall Rates from SSM/I Microwave Satellite Imagery, Final Report on Contract N000014-86-K-2001, University of Wisconsin-Madison, 45 pp.

Sadowski, A.F., 1979: Radar Guidance Program, NOAA Technical Procedures Bulletin No. 253, Silver Spring, MD, 14 pp.

Spencer, R.W., H.M. Goodman, and R.E. Hood, 1989: Precipitation Retrieval over Land and Ocean with the SSM/I: Identification and Characteristics of the Scattering Signal. *J. Atmos. Ocean Tech.*, **6**, 254-273.

Wakimoto, R.M., W. Blier, and C. Liu, 1991: A Radar Perspective of IOP 4 During ERICA, Research under Navy ONR Contract N00014-85-K-0630, UCLA, 6 pp.

Wilheit, T.T., and A.T.C. Chang, 1980: An Algorithm for Retrieval of Ocean Surface and Atmospheric Parameters from the Observations of the Scanning Multichannel Microwave Radiometer (SMMR), *Radio Science*, **15**, 525-544.

INITIAL DISTRIBUTION LIST

1. Defense Technical Information Center   2
   Cameron Station
   Alexandria, VA 22304-6145

2. Library, Code 0142   2
   Naval Postgraduate School
   Monterey, CA 93943-5002

3. Chairman (Code MR/Hy)   1
   Department of Meteorology
   Naval Postgraduate School
   Monterey, CA 93943-5000

4. Professor Carlyle H. Wash (Code MR/Wx)   3
   Department of Meteorology
   Naval Postgraduate School
   Monterey, CA 93943-5000

5. Professor Philip A. Durkee (Code MR/De)   1
   Department of Meteorology
   Naval Postgraduate School
   Monterey, CA 93943-5000

6. Capt Bayani J. Almario Jr., USAF   2
   Air Force Technical Application Center
   Patrick Air Force Base, FL 32925-5360

7. Commanding Officer   1
   AFIT/CIR
   Wright-Patterson Air Force Base, OH 45433-6583

8. Commander   1
   Air Weather Service
   Scott Air Force Base, IL 62225

9. Commanding Officer   1
    Air Force Global Weather Central
    Offutt Air Force Base, NE 68113-5000

10. USAF ETAC/LD   1
    Air Weather Service Technical Library
    Scott Air Force Base, IL 62225